Doctoral Thesis

Free Energy Landscape of Dipolar System: Statistical and Dynamical Analysis

Yohichi Suzuki

Department of Chemistry, Graduate School of Science,
Kyoto University

Acknowledgments

I could not have gotten to this point without the help of many peoples. First of all I would like to express my sincere gratitude to Prof. Yoshitaka Tanimura, for all his advices and encouragement during my years at Kyoto University.

During this period I have benefited from the help and support of many people. I am indebted to Prof. K. Ando, Dr. H. D. Kim, and Dr. M. Nishiyama of Kyoto University, Prof. A. Yoshimori, and Prof. R. Akiyama of Kyushu University, Prof. S. Saito of the Institute for Molecular Science, Prof. M. Maroncelli of Pennsylvania State University, Prof. J. Onuchic of the University of California San Diego and Prof. B. Bagchi of the Indian Institute of Science for our fruitful discussions and their useful comments.

I would like to thank all the present and former members of the Tanimura laboratory. In particular, Ms. Y. Ueno gave me a pleasant environment to study. I wish to thank Dr. A. Horikoshi, Dr. H. Kuninaka, Dr. Y. Nagata and Mr. A. Ishizaki for their kind help. The days we have passed together will remain a good memory forever. I wish to acknowledge my deep appreciation to Prof. Y. Fujitani of Keio University for his encouragement in research pursuits at Kyoto University.

I am grateful to all friends and, especially to my parents, Toshiki and Kazu Suzuki, for their constant moral support.

The research presented in this dissertation was supported by the research fellowship of Global COE program, International Center for Integrated Research and Advanced Education in Material Science, Kyoto University, Japan.

Last but not least, I would like to thank my wife Eriko for all her support and patience.

Contents

Chapter 1
General Introduction

1.1 Definition of Free Energy Landscape

Ensembles of atomic or molecular systems with competing interactions exhibit intriguing behaviors. In a glass and an amorphous solid, the long time relaxation processes play a major role as temperature lowered, leading to a slowing down and a broadening in the dynamical response.[1] The incomplete crystallization of polymers due to their topological connectivity and initial configuration makes the polymer chains fold back and forth to form crystalline lamellae.[2] Despite of complex energetics between a reactant and a product along with their surrounding solvent, electron transfer (ET) processes can be well characterized by the inverted parabolic dependence of ET rates as the function of energy gap.[3][4] Protein molecules fold into precise three-dimensional shapes under the entropic frustration associated with the chain connectivity.[5] Much of this complexity can be described and understood by taking a statistical approach to the energetics of molecular conformation, that is, to the free energy landscape (FEL). While the potential energy surface only deals with energetics, the FEL can deal with both the energetics and entropy.[6][7][8]

The FEL concept was introduced by Landau to explain a phase transition between liquid and crystal or between different crystal structures.[9] The FEL is a conformational substate of the free energy. For a macroscopic variable X, it is defined by

$$F(X) = -k_B T \ln Z(X), \tag{1.1.1}$$

where

$$Z(X) = \sum_{j \text{ for fixes } X} \exp\left[-E_j / k_B T\right] \tag{1.1.2}$$

is the partition function for fixed X. The Helmholtz free energy is then expressed as

$$F = -k_B T \ln\left[\int dX Z(X)\right]. \tag{1.1.3}$$

The function $F(X)$ is regarded as the constrained free energy with X. In the Landau case, X is the order parameter that represents the difference between the phases such as liquid and crystal. Although X is functionally important and is decidedly present, X is not necessary to be an externally controllable physical variable. In that sense, there are various ways of choosing X. The free energy and FEL are defined under the thermal equilibrium and $\exp\left(-F\left(X\right)/k_BT\right)$ corresponds to a probability which the macroscopic quantity of the system takes X. The definition of the FEL contains the thermal fluctuation, thus the FEL plays an important role in critical phenomena. Various mathematical techniques were developed to treat regular magnetic systems and spin glass systems.[10]. The basic assumption of this argument is that the system prefers to take the energy minimal of $F(X)$ from other metastable states. A state in different phases is explained by a local minimal point of $F(X)$, such as $F(X=1)$ for liquid phase and $F(X=0)$ for solid phase. In this sense, an analysis of $F(X)$ in phase transition explores the basins on the FEL rather than the entire structure of the FEL.

1.2 Dynamics on Free Energy Landscape

When system dynamics on free energy landscape (FEL) is discussed in terms of the entire structure of the FEL, a time-dependent Ginzburg-Landau (TDGL) approach is employed, where a driving force of X is assumed to be proportional to $dF(X)/dX$. This formalism was introduced to investigate dynamical phenomena of superconductors [11], and used to explain a motion of domain walls or interfaces.[12][13]

As the TDGL approach has been used successfully used to study critical phenomena, the FEL becomes important theoretical tools to analyze electron transfer (ET) reaction problems. In such problems, the FELs of the reactant and product states are expressed in terms of a reaction coordinate consisting of reactant and product along with their surrounding of solvent. Marcus evaluated the free energy of a given polarization and predicted the inverted parabolic or bell-shaped dependence of ET rates as the function of energy gap [3] , which was later observed experimentally.[14][15][16] A reaction coordinate could be adequately defined by the microscopic interaction energy [17][18][19][20] and a number of computer simulations were carried out to confirm the legitimacy of Marcus's theory.[21][22][23][24] At the present time, the FEL for ET processes is fairly understood at least for high-temperature cases and the interest of FEL analysis is shifting to a low temperature case, where the solvent motion freezes.[25] [26]

While the FEL of ET system was characterized by a simple parabolic shape, systems with involving complex interaction networks exhibit complex FELs depending on a choice of X. The examples are found in such systems as spinglass [10], glass [27][28], atomic cluster [29], polymers [30][31], and proteins [32][33][34][35][36][37], and indicate that a full understanding of the dynamical process requires a global overview of the FELs. Many basins corresponding to metastable states are exhibited in the systems and the dynamics among the basins is believed to govern the dynamical properties of the materials. Special attentions have been paid for protein folding problems, where the energy landscapes of protein have a single dominant basin and an overall funnel topography.[38][39]

Although the FEL analysis is proven to be a useful theoretical framework and is widely used to discuss the structure and dynamics of complex system, there are difficulties to investigate the dynamics at low temperature. The difficulties arise from the calculations for the FEL analysis; even in a small system, an enormous number of states need to be generated. For instance, for fifty two-level spins system, more than 10^{15} states must be generated for the calculation which cannot be handled by present computers. Several sampling methods were developed to simulate FEL for a large system [40][41], however the sampling procedures may truncate the dynamical pathways of the system and may differ the dynamical aspects especially at low temperature. The nature of FEL itself raises a fundamental question; the systems with different dynamics can have the same FEL. For example, a system described by either the Langevin dynamics [42] or Monte Carlo (Glauber dynamics) [43] can have the same FEL if the system part of the Hamiltonian is the same. Since the FEL is defined by the equilibrium state where dynamical behaviors become invisible, it is possible to consider the FEL and the dynamics are independent issues of discussions. From the experimental side, it is difficult to justify the validity of the FEL theory, since the FEL itself is not observable and, in addition, X is usually not experimentally controllable variable. A number of issues related with dynamical properties on FEL have been postulated. Our aim of this research is to clarify some of the problems mentioned above.

1.3 Modeling of System and Calculation of FEL

First of all, the property of the FEL needs to be investigated in a wide temperature range. One possible approach is to perform a full molecular dynamics (MD) simulation and to sample relevant states for a given temperature. However this approach is inappropriate for obtaining the FEL at low temperature, since the molecules consisting of the system have many degrees of freedom and the state of the system is trapped in the local energy minima. Thus we employ a simple model approach to reduce the degrees of freedom. For the protein folding problem, a freely jointed monomer chain model with simplified interactions is an example of the coarse graining for complex systems.[38][44][45][46][47] Several studies based on such model approach have been conducted to study static and dynamic aspects on solvation at high temperature. For example, the Brownian dipolar lattice model, which consists of point dipoles fixed on a simple cubic lattice [48][49], and the self-consistent continuum model in a spherical Onsager cavity[50], were used to investigate dielectric relaxation. Papazyan and Maroncelli introduced an ion in a Brownian dipole lattice to study ionic solvation.[51] Several theories for solvation dynamics [52][53] were developed and compared with computer simulations.[54][55][56] These models were sufficiently simple to apply for dynamical simulations, however, they still contain too many degrees of freedom to calculate the FELs especially at low temperature. Therefore we take a minimalist model approach for investigating the FEL, which was originally introduced by Onuchic and Wolynes to study glassy behavior of solvent molecules in electron and charge transfer reactions.[57] In this approach, ionic solvation on a polar solvent is modeled by a central charge surrounded by dipolar molecules with rotational dynamics represented by dipoles pointing only in two directions, the inward and outward directions relative to the ion as shown in Fig. 1.1. The simplicity of this model allows us to thoroughly explore how the energetics of solvation depend on solute charge, solvent dipole, and number of solvent molecules with an aid of random energy model (REM) theory, where the interaction energies among solvent molecules were assume to have a Gaussian distribution independent of the microscopic details of the molecular interactions.[58][59] Note that the approach based on the REM approximation was used for the protein folding problem by Bryngelson and Wolynes.[60] The minimalist model was also applied to investigate the dynamical phase transition [61][62] using Monte Carlo kinetics in addition to thermodynamic phase transition by utilizing the (mean) first passage time idea [63]. The extension of the minimalist model to multilayer solvent molecules with all dipole-dipole and charge-dipole interactions were applied to investigate the multiple glassy transitions associated with the freezing of the different solvent layers.[64]

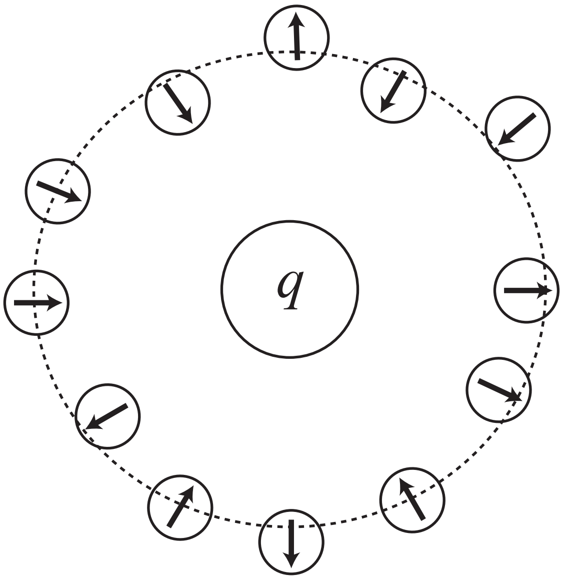

Figure 1.1: Minimalist model originally introduced by Onuchic and Wolynes. The ionic solvation on a polar solvent is modeled by a central charge surrounded by dipolar molecules with simple rotational dynamics represented by dipoles pointing only in two directions, the inward and outward directions relative to the ion. The translational motion of the surrounding dipoles is omitted and the dipoles are located on a single shell with random displacements.

For large systems, it is not appropriate to generate all states to calculate the FEL, because the huge number of states exists. Thus the sampling method is suitable, however it is expected that the state trapping in local minima occurs at low temperature using the Monte Carlo method with Metropolis algorithm [65] even if the degrees of freedom decrease. To overcome the difficulty, the generalized-ensemble algorithms [66] have been developed. The algorithms enable us to sample relevant states even in the low temperature case by using non-Bortzmann sampling weigh factors. One of the most well-known generalized-ensemble algorithms might be the multicanonical algorithm proposed by Berg and Neuhaus.[67][68] The entropic sampling [69][70], Wang-Landau sampling [71][72] and adaptive umbrella sampling [73] of the potential energy [74] also refer to the multicanonical algorithm. The generalized-ensemble algorithm has been applied to many problems such as spin glass, proteins and polymers.[75][76][77][78] Okumura and Okamoto suggested the multidimensional extensions of the multicanonical algorithm.[79][80] In Chapter 2, we explain the detail of the Wang-Landau algorithm.

1.4 Multidimensional Spectroscopy

For investigating the state dynamics on the FEL, we monitor the dynamics not only by linear absorption spectroscopy but also by multidimensional spectroscopy.[81] Since the multidimensional spectroscopy is proven to be a powerful tool for surveying molecular nature [82], several theoretical [83][84][85][86], experimental [87][88][89][90] and computational [91][92][93][94][95] efforts have been made to understand the manifold information for molecular motions and interactions. The multidimensional spectroscopy is the optical counterpart of multidimensional NMR[96] that can sensitively prove dynamical aspects of molecules in condensed phases. An observable in multidimensional vibrational spectroscopy is multibody correlation function of polarizability or dipole moment. The n-body correlation function is given as

$$C^{(n)}\left(t_{n-1},t_{n-2}\cdots,t_1\right)=\left\langle\left[\left[\left[\cdots\left[V\left(t_{n-1}\right),V\left(t_{n-2}\right)\right]\cdots\right],V\left(t_1\right)\right],V\right]\right\rangle \tag{1.4.1}$$

where $V(t)$ is the Heisenberg operator of V and $\langle\cdots\rangle$ represents the ensemble average. The operator V is the polarizability and the dipole moment for Raman and infrared (IR) spectroscopy, respectively. The three-body and four-body correlation functions are observed in the cases of fifth-order Raman and second-order IR and in those of seventh-order Raman and third-order IR, respectively. When a particle is driven by the harmonic potential and interacts with the external filed linearly, the three- and four-body correlation functions vanish because of the Gaussian integrals involved in the thermal average or cancellation of the coherence involved in the different Liouville paths. The multidimensional spectroscopy is sensitive to the anharmonisity and nonlinearity of system and is one of the available tools for investigating the microscopic details of the system such as mode-mode coupling [97][98][99][100] and dephasing mechanisms.[101][102][103][104][105] Note that the sensitivity is applicable not only to the kinetic systems following the quantum or classical dynamics, but also to the non-kinetic systems following the master equation or Smoluchowski equation.[106] The sensitivity of the multidimensional spectroscopy is fully taken into account when the dynamics is explored on different FELs.

1.5 Organization of This Thesis

In this thesis we introduce three types of models to investigate the properties of the FEL. In Chapter 2 we analyze a model for representing the ionic solvation which is the association of dipolar or ionic solvent molecules with a solute ion.[3] The model consists of a central charge surrounded by dipolar molecules posted on two-dimensional distorted lattice with simple rotational dynamics. Our interest is the structure of the FEL especially in the low temperature case. After obtaining the FEL for the ionic solvation system, we compare the results with the FEL given by employing a random energy model (REM) approximation.[58][59] We discuss how the structure of the FEL changes depending on the central charge in a wide temperature range.

In Chapter 3 we consider the FEL for the electron transfer system and introduce a model consists of a solute dipole surrounded by dipolar molecules with simple rotational dynamics located on the three-dimensional distorted lattice sites. The interaction energy between the solute and solvent dipoles as a reaction coordinate is adopted and the FELs are calculated by generating all possible states for a 26-dipolar-system and by employing the Wang-Landau sampling algorithm for a 92-dipolar-system. For the high temperature case the structure of the FEL is quadratic form, while for the low temperature case a notched structure appears on the FEL because of the complex interactions among solvent dipoles. The formation of the notched structure is analyzed with a statistical approach. The analysis indicates that the amplitude of the notched structure depend upon the segment size of the reaction coordinate and characterized by the interaction energy among dipoles. Using the simulated FEL, we calculate the reaction rates as a function of the energy gap for various temperatures.

In Chapter 4 a general purpose model for investigating the relationship between the FEL structure and relaxation dynamics is introduced. A dipolar crystal system is modeled by dipolar molecules posted on two-dimensional lattice sites with two-state librational dynamics. All dipole-dipole interactions are included to have frustrated interactions among the dipoles. To relate the FEL to the direct observable quantity, the reaction coordinate is chosen to be the polarization. For investigating dynamical aspects of the system, single flip and single-double mixed flips dynamics of dipoles are incorporated into the model with an aid of a master equation. The first- and third-order response functions of polarization, which are the observables of linear and two-dimensional (2D) IR or far IR spectroscopies, are calculated for different conditions characterized by the FEL. Since the profile of 2D IR spectroscopy is expected to detect the dynamics hidden in FEL, thus we are able to demonstrate the different dynamics following the Smoluchowski equation. The validity of the Smoluchowski equation approach to study the dynamics of system on the calculated FEL is also examined by calculating 1D and 2D signals to compare with the dynamics following the master equation.

In Chapter 5, we summarize this thesis and our conclusion is stated.

Chapter 2
Free Energy Landscape Analysis for Ionic Solvation System

2.1 Introduction

Ionic solvation is the process of attraction and association of solvent molecules with solute ions. Solvation plays an important role in many chemical processes in condensed phases such as electron and charge transfer reactions.[3][4] Complex dipolar interactions among solvent molecules cause the energy fluctuation which is necessary for thermally activated processes. To explore a role of solvation, one possible theoretical approach is to perform full molecular dynamics (MD) simulations by placing the charge in a collection of explicit solvent molecules. To have a fairly complete view of the solvent effect, one has to make an ensemble average over all possible trajectories of molecular motions. This approach is possible for high temperature case [107]; however, it is extremely difficult to apply for a low temperature case since the solvent molecules have too many degrees of freedom and there are too many local minima in the free energy landscape (FEL) at low temperatures. Despite of the complexity of the system, there is a still possibility to explain a role of solvent using a single macroscopic variable. For example, Marcus introduced a FEL as a function of a macroscopic variable representing the collective nature of the solvent molecules.[3] The solvent is treated as homogeneous dielectric continuum and the FEL is expressed as a quadratic function of the solvent polarization, which is adopted as the reaction coordinate for representing rearrangements of the solvent environment. Electron transfer (ET) rates are then evaluated in terms of the FELs for solvated reactants and products. The advantage of analyzing the system by means of the FEL is on the inclusion of entropic contributions upon the possible paths of chemical processes. For example, in electron transfer (ET) and charge transfer (CT) problems, a reaction rate may be calculated by averaging over all possible reaction paths with relevant statistical weight [19] [20] [21][22][23][24], since there are infinite numbers of reaction paths due to so many degrees of freedom arise from the solvent states. This procedure is almost impossible to carry out except for the high temperature case. The success of Marcus theory indicates that introducing a FEL is indeed an effective way to describe the reaction processes at least above the freezing temperature. Since the macroscopic variable may not be sensitive to the microscopic details of the interactions, we may employ a simple model to gain insight into a role of ionic solvation. For example, if we separate the rotational and translational degrees of freedom of solvent molecules, we can simplify the statistical analysis and facilitate construction of reliable energy landscapes at low temperatures. As mentioned in the Chapter 1, there are several studies based on such model approach suitable for studying dynamical aspects of solvation at high temperature, however they still contain too many degrees of freedom to calculate FELs. For this purpose, we take a minimalist model approach [57] and calculated the FELs as a function of the polarization.

The organization of this chapter is as follows. In section 2.2, a model composed of a single charge and dipolar solvent is described. The FEL is introduced as a function of a collective solvent variable. In section 2.3, the Wang-Landau algorithm is introduced to calculate the density of states as a function of energy and polarization. The numerical results are presented in section 2.4, and the final section is devoted to the conclusion.

2.2 Simulation Model for Ionic Solvation

The original minimalist model consists of a charged cavity and a single shell of solvent molecules represented by dipoles with simple rotational dynamics. These dipoles were allowed to point only two directions, inward to and outward from the charged cavity. Tanimura et al. extended the single shell of solvent molecules to two layers.[64] Monte Carlo simulations were carried out on this system including all dipole-dipole and charge-dipole interactions. We post the dipoles on a two-dimensional square lattice having lattice constant L and containing structural disorders (Fig. 2.1).

The position of the jth dipole $\mathbf{r}_j$ can be expressed using a lattice point vector $\mathbf{a}_j$ and displacement vector from the lattice point $\delta\mathbf{a}_j$, i.e., $\mathbf{r}_j = \mathbf{a}_j + \delta\mathbf{a}_j$. The strength and the unit vector specifying the direction of a dipole are μ and $\mathbf{S}_j$ respectively, where $\mathbf{S}_j = \mathbf{r}_j / |\mathbf{r}_j|$. If we introduce the sign operator $\sigma_j = \pm 1$, where the sign depends on whether the dipoles are pointing toward or away from the charge, the dipole movement is expressed as $-\mu\sigma_j\mathbf{S}_j$. Thus, the charge-dipole and dipole-dipole interactions are explicitly given by

$$E_{tot}\left(\{\sigma_i\}\right) = -\sum_{i=1}^{N} \xi_i(q)\sigma_i + \sum_{j=2}^{N}\sum_{k=1}^{j-1} J_{jk}\sigma_j\sigma_k \,, \tag{2.2.1}$$

where we set

$$\xi_i(q) = -\frac{\mu q}{r_i^2} \,, \tag{2.2.2}$$

and

$$J_{jk} = \mu^2 \frac{\mathbf{S}_j \cdot \mathbf{S}_k \left|\mathbf{r}_{jk}\right|^2 - 3\left(\mathbf{S}_j \cdot \mathbf{r}_{jk}\right)\left(\mathbf{S}_k \cdot \mathbf{r}_{jk}\right)}{\left|\mathbf{r}_{jk}\right|^5} \tag{2.2.3}$$

with $\mathbf{r}_{jk} = \mathbf{r}_j - \mathbf{r}_k$. The system exhibits a glassy behavior at various low temperatures because of these complex interactions with structural disorder. For the units of parameters, we employ values typical of ET or CT systems in polar solvents. Thus, q, μ and L are chosen to be 0.1 of the electron charge, the unit of Debye, and the unit of 2.1 $\overset{\circ}{\mathrm{A}}$, respectively. Adopting such typical units, the energy unit becomes 1.08×10^{-20} J, which is about 2.5($k_B T$) at room temperature. Then, simulations are carried out for $\mu = 1.85$ and $L = 1$ for different q and temperatures. The displacements from the lattice points obey a Gaussian distribution with average $\left\langle \delta\mathbf{a}_j \right\rangle = 0$ and standard deviation $\sqrt{\left\langle \delta\mathbf{a}_j{}^2 \right\rangle} = 0.1$. As a collective solvent coordinate, we introduce the total polarization defined by

$$p = n_- - n_+ \tag{2.2.4}$$

where n_+ and n_- represent the number of dipoles directed inward to and outward from the charged cavity, respectively, and the total number of dipoles are given by

$$N = n_- + n_+ \,. \tag{2.2.5}$$

We further introduce the average polarization per dipole defined by $x = p/N$. The FEL is then expressed in terms of x and T as

$$\frac{F(x,T)}{N} = -\frac{k_B T}{N} \ln \sum_{\{\sigma_i\} \in x} \exp\left(-E_{tot}\left(\{\sigma_i\}\right)/k_B T\right), \tag{2.2.6}$$

where the summation is taken over all configurations for which $x = x(\{\sigma_i\})$. Even in the present model which consists of a charged cavity and 80 dipoles on a 9×9 two-dimensional square lattice, there are too many states to enumerate all configurations in this summation. The procedures for efficiently sampling relevant states are essential in order to construct the FELs. Our approach is described in the following section.

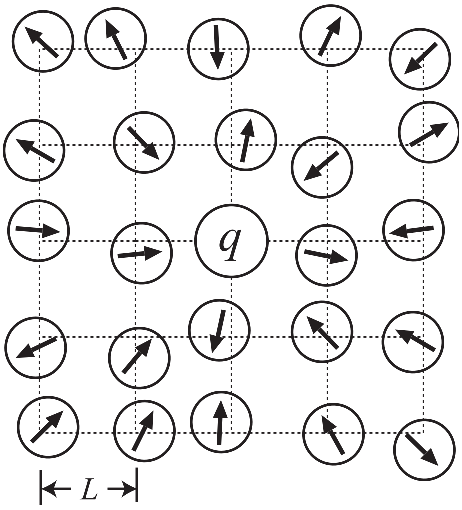

Figure 2.1: Schematic view of the solute and solvent model system. A solute molecule is represented by a point charge on the center of two-dimensional square lattice. Solvent molecules are expressed by dipoles located on disordered lattice sites surrounding the central charge. Each dipole is allowed to direct only two directions, toward and opposite to the central charge.

2.3 Wang-Landau Algorithm

The difficulty in evaluating Eq. (2.2.6) arises from the astronomically large number of states involved in the summation. Fortunately, such large number of states allows us to employ a statistical treatment. If we obtain a subset of the ensembles that are the representative of all of the states in the summation in Eq. (2.2.6), we may evaluate $F(x,T)$ from the subset. The Monte Carlo method with Metropolis algorithm[65] has been used to generate such representative ensembles, but this approach is time consuming for a glassy system at low temperature, because the trajectory of sampled states generated by the Monte Carlo method is easily trapped in the local energy minima. To overcome this difficulty, Berg and Neuhaus proposed the multicanonical algorithm [67][68], which has been applied to such problems in spin glasses, proteins and polymers.[75][76][77][78] The important aspect of this algorithm is the generation of a uniform sampling of configurations in energy space using artificial sampling weights instead of the Boltzmann weights. It means that the algorithm performs a random walk in energy space that allows the system to overcome energy barriers. From a set of sampling data, one can obtain thermodynamic averages at arbitrary temperatures and the calculation of the entropy and the free energy, both of which are associated with the partition function, is possible. Many researchers have attempted to improve the efficiency of such algorithms.[66][108] Recently an efficient algorithm for estimating the weight factors was developed by Wang and Landau.[71][72] This algorithm consists of two steps; the first step is obtaining the artificial weight factors by recursive updates, which enables us to get a flat histogram from the uniform sampling data in the energy space and the second step is generating configurations using such weight factors and calculating physical quantities by re-weighting probabilities to conform to the Gibbs ensemble. This algorithm is efficient for evaluating the free energy, but in order to calculate the FEL, which is a function of the polarization per molecule, an extension is necessary. We use the two-dimensional Wang-Landau algorithm to obtain the proper weighting factor not only for the energy space, but also for the polarization space. This algorithm enables us to obtain the FEL for all possible ranges of the polarization at any temperatures.

The outline of our procedure is as follows. First we introduce the weight factor $g(E,x)$ as a function of the energy E and the average polarization per dipole x. The transition probability from (E_1,x_1) to (E_2,x_2) is then defined by

$$p\big((E_1,x_1)\to(E_2,x_2)\big)=\min\left[\frac{g(E_1,x_1)}{g(E_2,x_2)},1\right], \tag{2.3.1}$$

where (E_1,x_1) and (E_2,x_2) refer to states before and after a single dipole is flipped. Next we introduce the histogram $H(E,x)$ defined by the number of visits made to each state (E,x). If we can make the histogram sufficiently flat using the transition rule (2.3.1), the density of states $n(E,x)$ will satisfy the following relation at arbitrary (E_1,x_1) and (E_2,x_2):

$$\frac{n(E_1,x_1)}{n(E_2,x_2)}=\frac{g(E_1,x_1)}{g(E_2,x_2)} \tag{2.3.2}$$

To obtain a flat histogram, first we set $g(E,x)=1$ for all possible ranges of energy and polarization. If the system attains to the states of energy E and polarization x for each time step during the update procedure Eq. (2.3.1), the weight factor is modified as $g(E,x)\to f_0 g(E,x)$ where f_0 is the modification factor set by $f_0=e\cong 2.71828$. If the transition $(E_1,x_1)\to(E_2,x_2)$ is rejected, we also modify the factor as $g(E_1,x_1)\to f_0 g(E_1,x_1)$. Iterating this update procedure yields the random walk in energy and polarization space and the modification of weight factors within the accuracy of f_0. When the histogram $H(E,x)$ becomes sufficiently flat, we update the modification factor f_0 as $f_1=\sqrt{f_0}$ and reset the histogram. In practice, it is not easy to obtain a perfectly flat histogram, thus if $H(E,x)$ for all possible E and x attains larger than 80% of the averaged value, $\langle H(E,x)\rangle$, we regard the histogram is flat. This procedure will be repeated for new modification factor f_i for $i>1$ with $f_i=\sqrt{f_{i-1}}$. The updating of f_i enables us to modify the weight factor more finely. We stop this iteration when $f_i<1.00000001$. After we obtain the weight factors to satisfy Eq. (2.3.2), we can normalize the density of states $n(E,x)$ using the condition

$$\sum_{E,x} n(E,x)=2^N. \tag{2.3.3}$$

Substituting Eq. (2.3.2) into (2.3.3) yields

$$n(E,x) = 2^N \frac{g(E,x)}{\sum_{E,x} g(E,x)}. \tag{2.3.4}$$

Finally, from Eq. (2.2.6), we have the expression of the FEL as

$$\frac{F(T,x)}{N} = -\frac{k_B T}{N} \ln\left(\sum_E n(E,x) \exp\left(-\frac{E}{k_B T} \right) \right). \tag{2.3.5}$$

In our simulation, we divide the regions of energy [-700,700] and polarization [-1.0,1.0] into 1401 and 81 segments, respectively. Since the directions of the dipoles are restricted to point inward to and outward from the central charged cavity, the periodic boundary conditions are not appropriate for our model. To avoid artificial errors from the boundary, we have used the open boundary condition. While we study the effects of the central charge upon the surrounding dipoles, we can suppress the influence of boundary dipoles by choosing a large lattice. The validity of the model can be easily checked by changing the lattice size.

2.4 Density of State and Free Energy Landscape

Following the procedure in the previous section, we have carried out simulations of a system composed of a charged cavity and 80 dipoles on the 9×9 two-dimensional square lattice with $\mu = 1.85$ and $L = 1$. In order to adjust the lattice size, we repeated the simulations for the 7×7 and 11×11 lattices and found that the properties of the FEL do not change qualitatively if the size is larger than 7×7. The displacements from the lattice points obeyed a Gaussian distribution with the average $\left\langle \delta \mathbf{a}_j \right\rangle = 0$ and the standard deviation $\sqrt{\left\langle \delta \mathbf{a}_j^{\,2} \right\rangle} = 0.1$. Using the two-dimensional Wang-Landau algorithm, we obtained the density of states (DOS) as the function of the energy E and the polarization x, $n(x,E)$, for different central charges $q = 0$ and 10 and the temperatures $T = 20$, 7 and 1. For comparison we also evaluated the average DOS, $\langle n(x,E) \rangle$, used in the random energy model (REM) theory, where all dipole-dipole and charge-dipole interactions are assumed to have a random Gaussian distribution function. Although the REM theory assumes the unrealistic interactions among the molecules, this allows us to obtain a handy analytical expression for a FEL.

The outline of the REM theory is explained in Appendix A. Note that, the theory may not predict the energy landscape properly at temperatures below the freezing point. Since a glassy system becomes frozen in low energy states such temperatures, the FEL has local minima in shape. However, since the theory averages over the local minima, the landscape is no longer a ragged function.

In order to adapt the REM theory to the simulation model, we set the two sets of parameters for the zero central charge, q=0, and the strong central charge, q=10. For the former set, the average charge-dipole interaction is set as $\bar{\xi}(q) = 0.0$, the dipole-dipole interaction $\bar{J} = -0.05$, and their standard deviations $\Delta\xi^2 = 0.0$ and $\Delta J^2 = 0.91$, while for the latter, the parameters are set respectively $\bar{\xi}(q) = -2.90$, $\bar{J} = -0.05$, $\Delta\xi^2 = 14.64$ and $\Delta J^2 = 0.91$.

We plot $\ln n(x, E)$ in Figs. 2.2(a) and 2.2(b), and $\ln\langle n(x, E)\rangle$ in Figs. 2.2(c) and 2.2(d) as contour maps for $q = 0$ and $q = 10$, respectively. In the peak region denoted by the solid lines, both the simulation and REM for $q = 0$ show symmetrical profiles, whereas (b) and (d) for $q = 10$ show unsymmetrical ellipsoidal profiles in the x-direction due to the energy difference between the inner and outer directions of dipoles arising from the charge-dipole interaction. For the low energy region $E < -200.0$, the distributions of $\ln\langle n(x, E)\rangle$ are always broader than those of $\ln n(x, E)$. This is because, to adapt to the simulation results, we have overestimated the width of a Gaussian distribution of the interaction energies used in the REM theory. The energy distribution from the simulation, which is not shown here, is characterized by the sum of narrower non-Gaussian peaks.

The free energy landscape (FEL) is calculated from Eq. (2.3.5). For comparison we also have evaluated the FEL for the REM case from

$$F_{\mathrm{REM}}\left(x,T\right)/N=\begin{cases}\dfrac{1}{N}\left(\bar{E}\left(x\right)-\dfrac{\Delta E^2}{2T}-TS^*\left(Nx\right)\right) & \text{for } T>T_c\left(x\right) \quad (2.4.1)\\[2ex] \dfrac{1}{N}\left(\bar{E}\left(x\right)-\Delta E\left(2S^*\left(Nx\right)\right)^{1/2}\right) & \text{for } T\le T_c\left(x\right) \quad (2.4.2)\end{cases}$$

with

$$S^*\left(Nx\right)=N\left[-\left(\frac{1+x}{2}\right)\ln\left(\frac{1+x}{2}\right)-\left(\frac{1-x}{2}\right)\ln\left(\frac{1-x}{2}\right)\right], \qquad (2.4.3)$$

by using the same parameters for the DOS calculation. (see Appendix A) The average solvation energy at polarization x and the standard deviation of the solvation energy are expressed as $\bar{E}(x)$ and ΔE, respectively. The FELs have two types of forms above and below a polarization-dependent phase transition temperature $T_c(x)$. Figures 2.3(a)-(c) show the FELs from the simulations (solid line) and the REM (dashed line) for zero central charge, $q=0$. Figures 2.3(d)-(f) show corresponding data for the strong central charge, $q=10$. The temperatures are set at $T=20$, 7 and 1, the dotted lines in Figs. 2.3 represent the fourth-order polynomial fits $F(x)=\sum_{j=1}^{4}a_j x^j$ in addition to a constant term.

The high temperature case, $T=20$ is shown in Figs. 2.3(a) and 2.3(d). This temperature satisfies $T>T_c(x)$ for the entire range of x and the REM results denoted by the dashed lines are calculated only from Eq. (2.4.1). The FEL from the simulation exhibits a similar profile as REM results. Both curves are parabolic for small $|x|$ as predicted by the Born-Marcus theory, but the curvature increases for large $|x|$ due to the entropic contribution. In the REM case, this contribution arises from $TS^*(Nx)$ in Eq. (2.4.1) where $S^*(Nx)$ is a logarithmic function of x. To illustrate the effects of the entropic contribution, we expand $F_{\mathrm{REM}}\left(x,T\right)/N$ in Eqs. (2.4.1) and (2.4.2) for small x as

$$\frac{F_{\mathrm{REM}}\left(x,T\right)}{N}=\begin{cases}-\left(\dfrac{\Delta E^2}{2TN}+T\ln 2\right)+x\bar{\xi}\left(q\right)+x^2\left(z\bar{J}+\dfrac{T}{2}\right)+x^4\left(\dfrac{T}{12}\right)+\cdots & T>T_c\left(x\right) \quad (2.4.4)\\[2ex] -\Delta E\sqrt{\dfrac{2\ln 2}{N}}+x\bar{\xi}\left(q\right)+x^2\left(z\bar{J}+\dfrac{\Delta E}{4}\sqrt{\dfrac{2}{N\ln 2}}\right)+x^4\left(\dfrac{\Delta E\left(3+4\ln 2\right)}{96\left(\ln 2\right)^{3/2}}\sqrt{\dfrac{2}{N}}\right)+\cdots & T\le T_c\left(x\right) \quad (2.4.5)\end{cases}$$

where z is the average number of dipoles interacting with each single dipoles.

As can be seen from Eq. (2.4.4), when the temperature becomes high, the contribution of the second-order coefficient as well as the fourth-order contribution increase. When a strong central charge is present, the dipoles tend to point outward to decrease the energy. In the case, the term proportional to x in Eq. (2.4.4) also plays a role in the REM case, the minimum point of landscape shifts to the positive direction. In the simulation case, there is also a cubic contribution to the FEL. The fitting function now involves all terms as $F(x)=\sum_{j=1}^{4} a_j x^j$. The lack of the cubic term in the REM case is due to the oversimplification of charge-dipole interactions. In the simulation model, the intensity of the charge-dipole interactions change depending on the location of dipoles, which makes the FEL a complex function of the polarization. In contrast, the REM theory assumes a spatially uniform interaction which makes the free energy a linear function of the polarization.

Figs. 2.3(b) and 2.3(e) show the intermediate temperature cases, $T = 7$. The REM results in the region of $|x| < 0.8$ for Fig. 2.3(b) and $|x| < 0.6$ for Fig. 2.3(e) are calculated from Eq. (2.4.1) to satisfy $T > T_c(x)$, whereas those in the remaining regions are calculated from Eq. (2.4.2). The FELs calculated by the REM are broader than the simulated ones, especially in the region around $x = 1$ and $x = -1$. As illustrated in Fig. 2.2, this can be explained by the fact that a profile of the lower part of average DOS is always broader because of the overestimation of energy distribution. In the same manner as in the high temperature case, the FELs can be well fitted by a polynomial function. As the temperature lowers, the fourth-order contribution of the fitting curves becomes large as is illustrated by the REM theory. For the fixed parameter $z\bar{J} = -1.8$, the ratio a_4 / a_2 in Eq. (2.4.4) increases with decreasing temperature up to $T = 3.6$.

Figs. 2.3(c) and 2.3(f) show the results for the low temperature case, $T = 1$. The REM results are calculated from Eq. (2.4.2), since this temperature meets $T < T_c(x)$ for the entire range of x . At this very low temperature, the simulated FELs are no longer smooth due to the presence of multiple local minima arising from the frustrated interaction among the dipoles. This roughness can be clearly distinguished from the numerical errors of the simulations, since the errors in these calculations are less than the line width in Fig. 2.3.

Notice that the roughness depends upon the disorder of the dipoles. Thus, if we make the ensemble average of the FELs for different configurations of dipoles, this roughness may be smoothed over. On the contrary, the landscape for the REM is smooth even at the low temperature, since the REM assumes the smooth Gaussian function for the average DOS.

The profile of the FEL as shown in Fig. 2.3(c) is expressed by a quartic function $F(x) \approx a_4 x^4$, instead of the parabolic function except for the small roughness of the lines. On the other hand in Eq. (2.4.5), the contribution of the parabolic term compared with quartic term is not negligible as $a_2 / a_4 = 0.75$ for $z\bar{J} = -1.8$. Thus the quartic profile of the FEL can not be explained only by the entropic contribution. Since the dipole-dipole interactions are assumed to be Gaussian random variables, the complex interactions depending on the position of dipoles are not considered in the REM theory. Moreover the average energy at polarization x is given by the parabolic form. The fact that the strong quartic dependence of the FEL is observed at the low temperature suggests that the average energy contains a quartic term due to the spatial correlation among dipoles.

Fig. 2.3(f) illustrates the energy landscape for the strong central charge of $q = 10$. In addition to the parabolic and quartic contributions of x, the REM case exhibits the linear contribution, i.e., $F(x) \approx a_1 x + a_2 x^2 + a_4 x^4$, whereas for the simulation case exhibits the linear and cubic contributions, i.e., $F(x) \approx a_1 x + a_2 x^2 + a_3 x^3 + a_4 x^4$. As explained in the Fig. 2.3(d), both the linear and cubic contributions arise from the charge-dipole interactions. Indeed, they appear even when we calculated the FEL for the model without the dipole-dipole interactions (not shown).

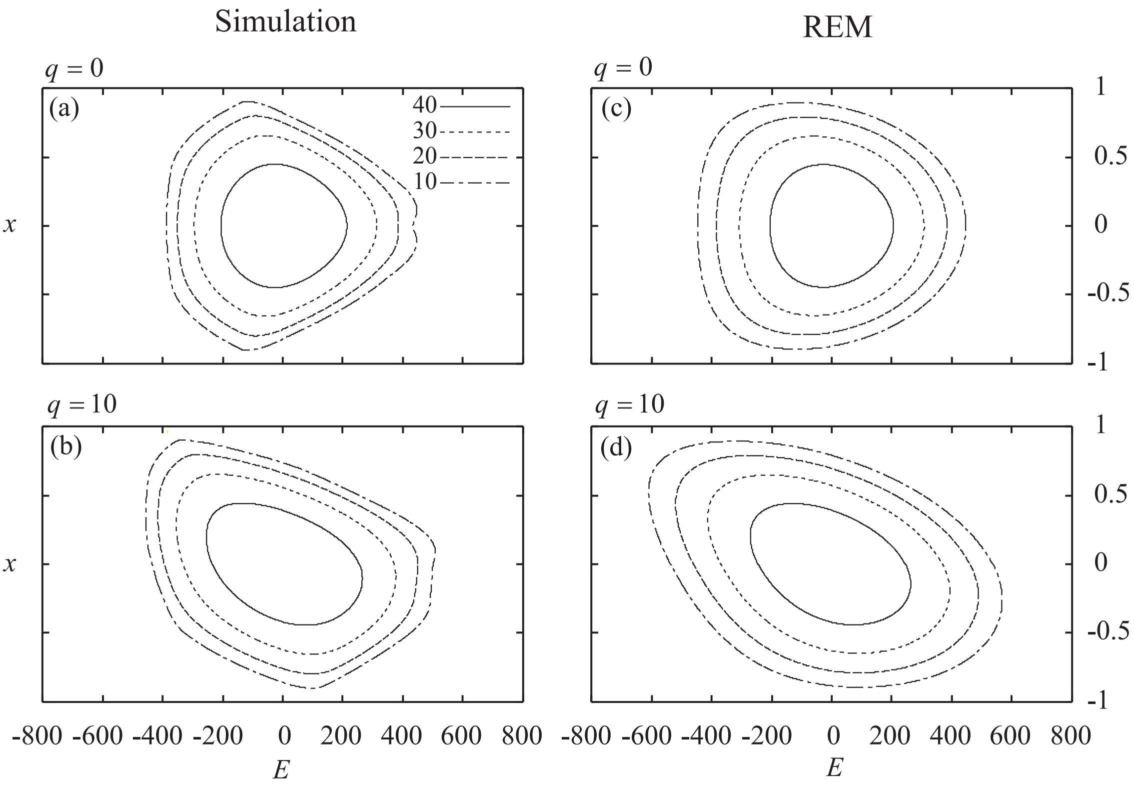

Figure 2.2: Counter maps of the logarithms of the density of states are plotted for the cases of (a) no central charge $q = 0$ and (b) strong central charge $q = 10$. For comparison, the logarithms of the average density of states used in the REM approximation are also plotted as contour maps for the cases of (c) no central charge q=0 and (d) strong central charge q=10.

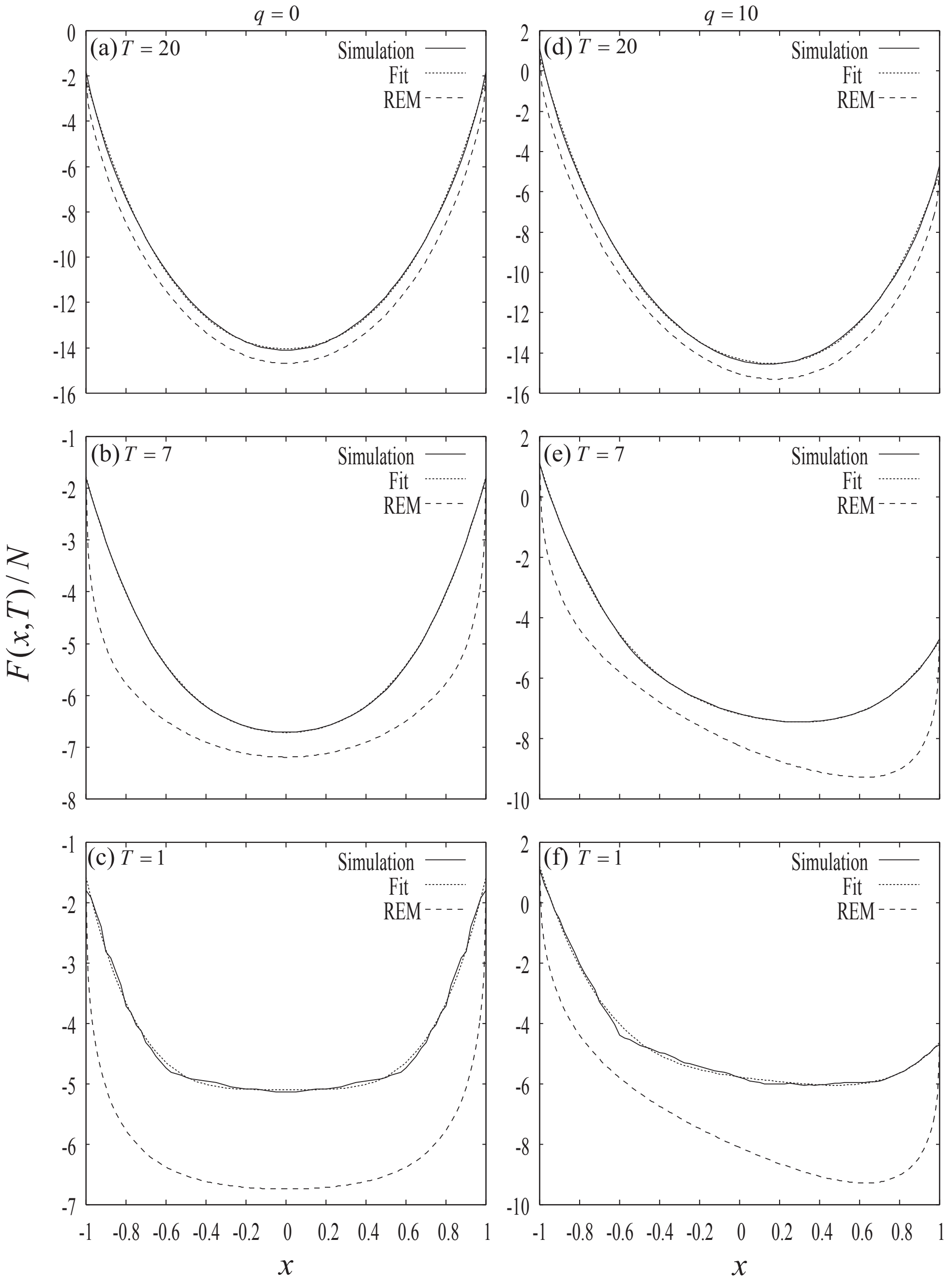

Figure 2.3: FELs as the function of the polarization in the cases of no central charge $q=0$, (a)-(c), and strong central charge $q=10$, (d)-(e) for different three temperatures, $T=1$, $T=7$ and $T=20$. The solid, dotted and dashed lines represent the results of our simulation, fourth-order polynomial fitting and the REM, respectively.

2.4 Conclusion

We calculated the free energy landscape (FEL) as a function of polarization for a two-dimensional charge-dipole lattice model using the Wang-Landau algorithm. To elucidate the entropic contributions to the free energy, we supplemented the calculations using the random energy model (REM) approach by taking the parameters from the simulation model. In the high temperature case without a central charge, the FELs calculated from the simulation and REM are parabolic in shape for small polarizations, as the Born-Marcus theory predicts. In the large polarization region, both the simulated and the REM results also include a small quartic contribution that arises from the entropic term in the definition of the free energy as pointed out by Onuchic and Wolynes.[57]

For the strong central charge, the FEL becomes asymmetric as a result of charge-dipole interactions. In addition to the quadratic and quartic terms, the FEL is fitted by linear and cubic terms in the simulation case whereas by a linear term only in the REM case, because the REM theory oversimplifies the form of the charge-dipole interactions.

When the temperature decreases, the difference between the simulation and REM results becomes pronounced. This can be explained more clearly when we plot the density of states (DOS) as a function of both energy and polarization. The REM results exhibit a broad DOS due to the overestimation of the interaction energies chosen to adjust the simulation model to the REM theory. In the low temperature case, the FEL observed in the simulations is no longer smooth. The roughness arises from the inhomogeneous charge-dipole and dipole-dipole interactions and depends upon the positions of the dipoles. By ignoring this roughness, the profile of the FEL is fitted by a polynomial function up to the fourth-order of the polarization. As in the high temperature case, the linear and cubic contributions appear when the strong central charge is introduced.

In this Chapter we have calculated the FELs for a system composed of a charged cavity and dipoles which are restricted to point only to two directions. The present model is too simple to describe many important effects involved in solvation dynamics, such as librational motion. Generalization to a realistic model with the large degrees of freedom in three-dimensional space is necessary to explore the universality of our results. Thermal as well as dynamical aspects of such system are important to relate the FEL to real experiments of a relaxation.

Chapter 3
Free Energy Landscape Analysis for Electron Transfer System

3.1 Introduction

The free energy landscape (FEL) of electron transfer (ET) system is of fundamental importance to account for ET rates in solvent as recognized by Marcus.[3][4] In this context, the FELs of the reactant and product are expressed in terms of a reaction coordinate consisting of reactant and product along with their surrounding of solvent. Marcus evaluated the free energy of a given polarization and calculated the ET reaction rates as

$$k \sim \exp\left(-\frac{(\lambda + \Delta G)^2}{4k_B T\lambda} \right) \tag{3.1.1}$$

where λ and $-\Delta G$ are the reorganization energy and the energy gap, respectively. From the above expression, the energy gap law, Marcus has predicted that the inverted parabolic or bell-shaped dependence of ET rates as the function of energy gap, which indicates the ET rates increase in the small energy gap region (the normal region), whereas they decrease in the large energy gap region (the inverted region). His expression was based on a continuum dielectric model of solvent and thus the molecular aspects of the solvent were missing.

Although Marcus's theory explained the energy gap dependence reasonably well [14][15][16], such macroscopic continuum model is not sufficient to describe ET processes especially for dynamics of solvent.[109] The FELs of the macroscopic dielectric system were given by a functional form of polarization.[4][110] To calculate the FELs using models based on the microscopic molecular details, one has to define relevant reaction coordinates. Taking statistical mechanics approach, Marcus has explored ways to abstract small dimensional coordinates from the multidimensional phase space using the technique of equivalent equilibrium distribution.[111] His idea was later developed and utilized for the calculation of the ET rate by computer simulations.[112] Calef and Wolynes showed that a reaction coordinate could be adequately defined by the microscopic interaction energy [17][18], and several computer simulations were carried out using the reaction coordinate which has the energy dimension to confirm the legitimacy of Marcus's theory.[21][22][23][24] An expression of the free energy in terms of molecular distribution function including dipole interactions was also given by using a density functional theory.[113][114]

Here, we introduce a factor $f(\{R_i\})$ for configuration coordinates of solvent $\{R_i\}$ as

$$f(\{R_i\}) \equiv E^R(\{R_i\}) - E^P(\{R_i\}), \tag{3.1.2}$$

where $E^i(\{R_i\}) \equiv E^i_{d-s}(\{R_i\}) + E^i_{s-s}(\{R_i\})$ is the interaction energy for reactant ($i = R$) or product ($i = P$) consisting the solvent-solute interaction energy, $E^i_{d-s}(\{R_i\})$, and solvent dipole-dipole energy $E^i_{s-s}(\{R_i\})$.[19][20] If we define the FELs of reactant and product by

$$G^i(x,T) = -k_B T \ln\left(\int dR_1 \cdots dR_N \delta\left(x - f\left(\{R_i\}\right)\right) \exp\left(-E^i\left(\{R_i\}\right)/k_B T\right)\right), \tag{3.1.3}$$

the free energies of the reactant and the product satisfy the relation,

$$G^R(x,T) = x + G^P(x,T). \tag{3.1.4}$$

Suppose if the FEL is expressed in a quadratic form as

$$G^R(x,T) = ax^2 + bx, \tag{3.1.5}$$

the ET rates are then evaluated as Eq.(3.1.1), in which $-\Delta G$ is the energy gap between the two surfaces and $\lambda = 1/4a$.

At present, the FEL for ET processes is fairly understood at least for the high-temperature case, where the FEL is well approximated by the parabolic function. At low temperature, however, it is difficult to calculate the reaction rates, since the solvent molecules have enormous degrees of freedom and there are too many local minima that trap molecular motions to acquire the reliable FELs. In order to deal with such problem, a simple model is often introduced to reduce the degrees of freedom as mentioned in Chapter 1. To study a possible role of solvent molecules influencing the electron transfer (ET) or charge transfer (CT) reaction rates in glassy phase, we have utilized the minimalist model approach.[57]

In this chapter, a survey of the FELs for the extended minimalist model as the function of x defined by Eqs. (3.1.2) and (3.1.3) at temperatures below and above the freezing point. In Sec. 3.2, we describe the model and the reaction coordinate. In Sec. 3.3, the FELs for different temperatures are numerically calculated by generating all possible states for a 26-dipolar-system and by employing Wang-Landau sampling algorithm for a 92-dipolar-system. From the calculated FELs, the ET reaction rates are also evaluated. The final section is devoted to the conclusion.

3.2 Simulation Model and Reaction Coordinate

To adapt minimalist model for ET reaction process, we have replaced the central charged cavity by a solute dipole moment. Then we configure the solvent dipoles around the solute dipole on the three-dimensional distorted lattice with the lattice constant L. We have treated all solute-solvent and solvent-solvent interactions explicitly, whereas they were assumed to be random Gaussian interactions in the original minimalist model with the random energy model (REM) analysis. The schematic view of our modified model is depicted in Fig. 3.1. The solute dipole moment is represented by $\mathbf{z}\mu_d^i$, where $\mathbf{z}$ is the unit vector in the z direction and μ_d^i denotes the magnitude of the solute dipole for the reactant ($i = R$) and the product ($i = P$). We denote the position of each solvent dipole as $\mathbf{r}_j = \mathbf{a}_j + \delta\mathbf{a}_j$, where $\mathbf{a}_j$ is the jth lattice point vector and $\delta\mathbf{a}_j$ is the random displacement from the lattice point. The magnitude and the direction of the jth solvent dipole is denoted by μ_{solv} and the unit vector $\mathbf{S}_j$, respectively, where $\mathbf{S}_j = \mathbf{r}_j / |\mathbf{r}_j|$. If we introduce the sign operator $\sigma_j = \pm 1$, where the sign depends on whether the dipoles are pointing toward or away from the solute dipole, the dipole movement is expressed as $-\mu_{solv}\sigma_j\mathbf{S}_j$. Thus all the interactions among solute and solvent dipoles are expressed as

$$E^i\left(\mu_d^i, \boldsymbol{\sigma}\right) = E_{d-s}^i\left(\mu_d^i, \boldsymbol{\sigma}\right) + E_{s-s}\left(\boldsymbol{\sigma}\right). \tag{3.2.1}$$

Here, the energy of the solute-solvent and the solvent-solvent dipoles are defined by

$$E_{d-s}^i\left(\mu_d^i, \boldsymbol{\sigma}\right) = \sum_{j=1}^{N} g_j\left(\mu_d^i\right)\sigma_j \tag{3.2.2}$$

and

$$E_{s-s}\left(\boldsymbol{\sigma}\right) = \sum_{j=2}^{N}\sum_{k=1}^{j-1} h_{jk}\sigma_j\sigma_k\ , \tag{3.2.3}$$

respectively, where

$$g_j\left(\mu_d^i\right) = -\mu_{solv}\mu_d^i \frac{\mathbf{S}_j \cdot \mathbf{z}\left|\mathbf{r}_j\right|^2 - 3\left(\mathbf{S}_j \cdot \mathbf{r}_j\right)\left(\mathbf{z}\cdot\mathbf{r}_j\right)}{\left|\mathbf{r}_j\right|^5} \tag{3.2.4}$$

and

$$h_{jk} = \mu_{solv}^2 \frac{\mathbf{S}_j \cdot \mathbf{S}_k\left|\mathbf{r}_{jk}\right|^2 - 3\left(\mathbf{S}_j \cdot \mathbf{r}_{jk}\right)\left(\mathbf{S}_k\cdot\mathbf{r}_{jk}\right)}{\left|\mathbf{r}_{jk}\right|^5} \tag{3.2.5}$$

with $\mathbf{r}_{jk} = \mathbf{r}_j - \mathbf{r}_k$, and N is the total number of solvent dipoles This system exhibits a glassy behavior at the low temperatures because of the complex interactions among the solvent dipoles with the structural disorder. We chose values typical of ET or CT systems in polar solvents as $\mu_{solv} = 1.85$ and $L = 1$ in the unit of Debye and the unit of 2.1 Å, respectively. The characteristic energy is then evaluated as $\Delta U = 1.08\times10^{-20}$ J, which is about 2.5($k_B T$) at room temperature. We employ two types of system: one is $3\times3\times3$ lattice sites and the other is $5\times5\times5$ lattice, but we omit four dipoles on each corner of the lattice for later system due to the limitation of our CPU power. Thus, we used a total of 26 and 92 dipoles for their calculations. We utilize the open boundary condition to avoid undesired effects arise from the treatment of boundary. The displacements from the lattice points obey a Gaussian distribution with average $\left\langle \delta\mathbf{a}_j \right\rangle = 0$ and standard deviation $\sqrt{\left\langle \delta\mathbf{a}_j{}^2 \right\rangle} = 0.1$.

For our model, we rewrite Eq. (3.1.2) as

$$f\left(\boldsymbol{\sigma}\right) = E^R\left(\mu_d^R, \boldsymbol{\sigma}\right) - E^P\left(\mu_d^P, \boldsymbol{\sigma}\right). \tag{3.2.6}$$

The FELs of the reactant ($i = R$) and the product ($i = P$) are calculated from

$$G^i\left(x,T\right) = -k_B T \ln \frac{1}{C} \sum_{|f(\boldsymbol{\sigma})-x|<\Delta x} \exp\left(-\frac{E^i\left(\mu_d^i, \boldsymbol{\sigma}\right)}{k_B T} \right). \qquad (3.2.7)$$

Here, the summation has taken over all configurations for which $f(\boldsymbol{\sigma})$ takes a value between $x - \Delta x/2$ and $x + \Delta x/2$, where Δx is the segment (mesh) size of the reaction coordinate. We introduce the dimensionless constant C to adjust the position of $G^i(x,T)$. When we set C to be proportional to Δx, the position of the energy landscape of various segment sizes can be fixed if the assigned temperatures are the same. In the following calculations, we set $C = \Delta x / \Delta U$, where $\Delta U = 1.08 \times 10^{-20}$ J is the characteristic energy of the system. In Eq. (3.2.7), we adopt $\mu_d^R = 0$ and $\mu_d^P = 2$ for a situation: a neutral solute is surrounded by the solvent in the reactant state and the ET reaction occurs then is polarized.

For the 26-dipolar-case, we evaluate Eq. (3.2.7) by generating all configurations of $\boldsymbol{\sigma}$ and classifying $f(\boldsymbol{\sigma})$ in the range $x_i - \Delta x/2 \le f(\boldsymbol{\sigma}) < x_i + \Delta x/2$ for *i*th segment x_i, which satisfies $\Delta x = x_{i+1} - x_i$. Although we can obtain the exact FEL for any Δx in such small system, we cannot generate all configurations by any means for a large system. For example, a system with 92 dipoles involves enormous degrees of freedom even with directional restrictions of the dipoles ($\sim 2^{92}$). Thus, it is essential to sample relevant states for constructing the FEL, and then to use the Wang-Landau algorithm explained in Chapter 2. We employ the reaction coordinate x defined in Eqs. (3.2.6) and (3.2.7) instead of the polarization and adapt the two-dimensional Wang-Landau algorithm to calculate the FEL. The parameters or conditions used in the algorithm are shown as follows.

When the histogram $H(E,x)$ defined by the number of sampled states (E,x) attains larger than 70% of the average value, $\langle H(E,x) \rangle$, for all possible ranges, we regard the sampling as having been done uniformly in the energy and reaction coordinate space. In order to generate the sampling weight, we divide the regions of energy -2000< $E/\Delta U$ <2000 and reaction coordinate -100< $x/\Delta U$ <100 into 4001 and $(200\Delta U / \Delta x)+1$ segments, respectively. We generate the density of states (DOS) after obtaining the artificial weight factors by recursive updates which enables us to obtain a flat histogram of the uniform sampling data in the energy and reaction coordinate spaces. We then calculate the FEL as the function of x by re-weighting probabilities to conform to the Gibbs ensemble.

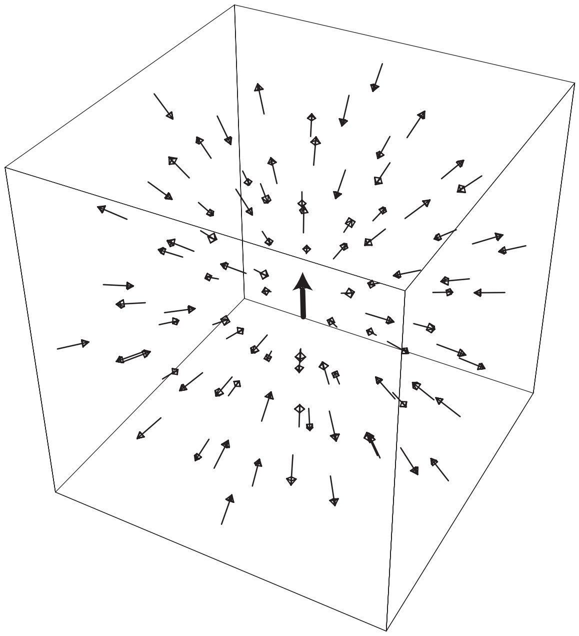

Figure 3.1: A schematic view of a solute and solvent model. A solute molecule is represented by a dipole on the center of three-dimensional square lattice. Solvent molecules are expressed by dipoles located on the disordered lattice sites surrounding the central dipoles. Each solvent dipole is allowed to direct only two directions, toward and opposite to the central dipole.

3.3 Results and Discussion

A. Free Energy Landscapes of a 26-Dipolar-System

Figures 3.2 (a)-(d) illustrate the free energy landscapes (FELs) of a distorted $3\times3\times3$ square lattice system with 26 dipoles for different temperatures and segment sizes: (a) $T=10$ and $\Delta x=10^{-1}$, (b) $T=1$ and $\Delta x=10^{-1}$, (c) $T=10$ and $\Delta x=10^{-3}$, and (d) $T=1$ and $\Delta x=10^{-3}$ in the unit of $\Delta U=1.08\times10^{-20}$ J. Here and hereafter we set $k_B=1$. We have analyzed the temperature dependence of the heat capacity and found a sharp peak at $T_c\approx2$ that corresponded to the freezing temperature of dipolar rotational motions. Thus the cases for (b) and (d) are in a glassy state. These landscapes are directly calculated from Eq.(3.2.7) by generating all possible dipolar states numerically and are not obtained from the Wang-Landau approach. Such exact calculations can be carried out only for a small system with 2^{26} dipolar configurations. Since this system is too small to extract reasonable free energy profiles, we have observed a change of curvature around $|x/N|=0.2$ as an artifact of the small system. We have used these results to analyze the segment size of the reaction coordinate, which has to be introduced to calculate the free energy of larger systems.

While the FEL becomes smooth at high temperature as illustrated in Fig. 3.2(a), it exhibits the small notched structure (roughness) on the profile at low temperature as in Fig. 3.2(b). This feature can be explained from the distribution of states as a function of reaction coordinate *x* and energy *E* as schematically depicted by dots in Fig. 3.3. At the high temperature, all states in the segment between $x_i-\Delta x/2$ and $x_i+\Delta x/2$ contributes to $G^R\left(x_i,T\right)$, while only the lower energy part of states in the segment contributes to $G^R\left(x_i,T\right)$ at the low temperature due to the Boltzmann factor in Eq.(3.2.7) as indicated with solid line in Fig. 3.3. Since the number of states is sparse in the lower energy region, $G^R\left(x,T\right)$ changes rapidly as the function of *x* depending on the position of the low energy states. This feature becomes prominent especially for small Δx, where only a few states can take part in for calculations of $G^R\left(x_i,T\right)$. In this case, as shown in Fig.3.2(c), we have also observed the notched profiles of the landscape even at the high temperature.

Using the exact distribution of states, we analyzed the statistics of the notched structure. First, we extrapolate the profiles of the FEL up to sixth-order using the fitting function $G^R_{fit}(x) = \sum_{k=0}^{3} a_i (x/N)^{2k}$ for the range $|x/N| \leq 0.2$. Due to the conditions of $f(\boldsymbol{\sigma}) = -f(-\boldsymbol{\sigma})$ and $E^R(\mu^R_d, \boldsymbol{\sigma}) = E^R(\mu^R_d, -\boldsymbol{\sigma})$, $G^R(x,T)$ is symmetric with respect to $x = 0$ and the polynomial function does not contain the odd-order terms. Then we subtract $G^R_{fit}(x)$ from $G^R(x,T)/N$ and obtain the notched part of free energy as $\delta G(x_i) = G^R(x_i,T)/N - G^R_{fit}(x_i)$, where x_i is the value of the reaction coordinate at *i*th segment which satisfies $\Delta x = x_{i+1} - x_i$. $G^R(x,T)/N$ for $T = 1$ and $\Delta x = 10^{-2}$ is depicted in Fig. 3.4 with solid line and the fitted line is with the dashed line, in which the fitting parameters are $a_6 = 6731.75$, $a_4 = -307$, $a_2 = 3.9$ and $a_0 = -2.26$. The inset of Fig. 3.4 shows the histogram of $\delta G(x_i)$ and the fitted normal distribution with dashed line where the average and the standard deviation are $\overline{\delta G} = 0.0$ and $\sqrt{\overline{\delta G^2}} = 0.098$, respectively. In the small region of *x*, where the Gaussian fitting works well, the sequence of $\delta G(x_i)$ is uncorrelated at the different x_i, and thus $\delta G(x_i)$ can be regarded as the white noise with respect to x_i.

Calculated $\sqrt{\overline{\delta G^2}}$ as the function of temperature for different Δx is plotted in Fig. 3.5. The amplitude $\sqrt{\overline{\delta G^2}}$ tends to be large for small Δx, since the number of the states involved in the free energy calculations becomes small and the statistical deviation becomes large. For $T < 10$, the amplitude becomes large for small T, since only lower energy states in the segment can contribute to the free energy calculations due to the Boltzmann factor in Eq. (3.2.7). At very low T, the lowest energy state in the segment dominate the free energy and thus we have $G^R(x_i,T) \approx E^{\min}_i$, where $E^{\min}_i$ is the lowest energy in the *i*th segment and therefore the FELs becomes temperature independent. For $T > 10$, $\sqrt{\overline{\delta G^2}}$ increases as the temperature increases. At such high temperature, the Boltzmann factor play a lesser role and thus the total number of states, $n(x_i)$, in the *i*th segment determines the value of the free energy as $-k_B T \ln n(x_i)$. Since $n(x_i)$ may change rapidly for small Δx, the amplitude will also change.

In Fig. 3.6, we plot $\sqrt{\overline{\delta G^2}}/\Delta U$ as the function of $\Delta x/\Delta U$ for different temperatures, where ΔU is the characteristic energy scale for the system. The calculated results can be well fitted by the linear functions in the logarithmic scales. This indicates that we can always extrapolate their amplitudes $\sqrt{\overline{\delta G^2}}$ from the values in large Δx.

Since the lowest energy $E_i^{\min}$ determines the free energy in the individual segments especially for the low temperature case, the differences of the lowest energy among the different segments give rise to the notched structure. To see this point more clearly, we consider the change of the total energy and the reaction coordinate by flipping one dipole while others being fixed. The energy of the k th dipole is evaluated as

$$\begin{aligned}\Delta E(\sigma_k \to -\sigma_k) &= -2\sum_{j\neq k} h_{kj}\sigma_k\sigma_j \\ &\approx -2\bar{h}\sigma_k\sum_{j\neq k}\sigma_j\end{aligned}, \qquad (3.3.1)$$

where the interaction parameter h_{kj} is approximated by their mean value $\bar{h}$ defined by

$$\bar{h} \equiv \frac{1}{N}\sum_{k=1}^{N}\left(\frac{1}{N-1}\sum_{j\neq k} h_{kj}\right). \qquad (3.3.2)$$

Similarly, the change of the reaction coordinate by flipping one dipole is given by

$$\begin{aligned}\Delta x(\sigma_k \to -\sigma_k) &= 2g_k\left(\mu_d^P\right)\sigma_k \\ &\approx 2\bar{g}\sigma_k\end{aligned}, \qquad (3.3.3)$$

where the solute-solvent interaction parameter $g_k\left(\mu_d^P\right)$ is approximated by their mean value

$$\bar{g} = \frac{1}{N}\sum_{k=1}^{N} g_k\left(\mu_d^P\right). \qquad (3.3.4)$$

If all configurations of $\{\sigma_1,\cdots,\sigma_{k-1},\sigma_{k+1},\cdots\sigma_N\}$ occur with the same probability, $1/2^{N-1}$, the fluctuation (standard deviation) of the total energy and reaction coordinate by flipping one dipole are given by

$$\Delta E_{flip} = 2\left|\overline{h}\right|\sqrt{(N-1)}\,, \tag{3.3.5}$$

and

$$\Delta x_{flip} = 2\left|\overline{g}\right|, \tag{3.3.6}$$

respectively. For the 26-dipolar-system, they are evaluated as $\overline{h} = 0.9$ and $\overline{g} = 0.05$, and we have $\Delta x_{flip} = 0.1$ and $\Delta E_{flip} / N = 0.3$. These values are roughly in accordance with the relation in Fig. 3.6, which indicates that the amplitude of the notched structures relates to the flipping energy and the corresponding change of the reaction coordinate. We should also notice that although the true FELs have the notched structures whose scale is much smaller than Δx_{flip}, a real transition may occur only through the flipping of dipoles. Therefore the structure smaller than Δx_{flip} on the FELs may not affect reaction processes.

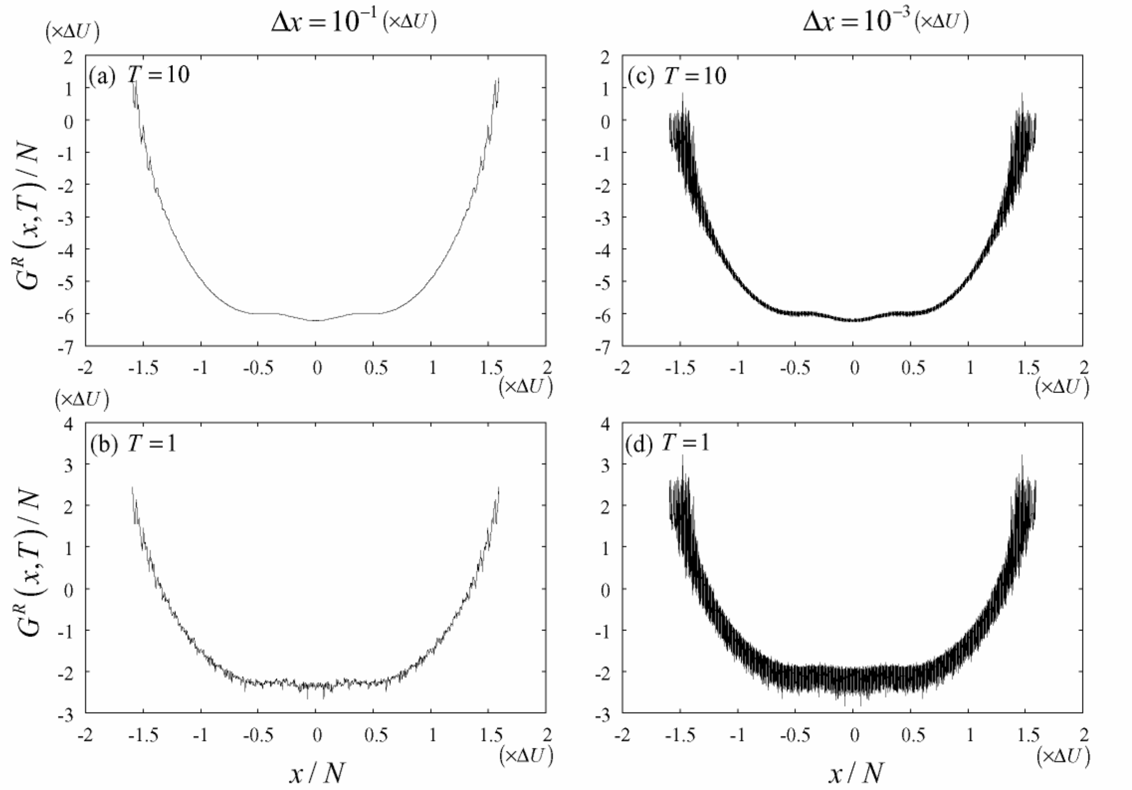

Figure 3.2: The free energy landscapes of a distorted $3 \times 3 \times 3$ square lattice system with 26 dipoles for different temperatures T and segment sizes Δx: (a) $T = 10$ and $\Delta x = 10^{-1}$, (b) $T = 1$ and $\Delta x = 10^{-1}$, (c) $T = 10$ and $\Delta x = 10^{-3}$, and (d) $T = 1$ and $\Delta x = 10^{-3}$. T and Δx are measured in the unit of $\Delta U = 1.08 \times 10^{-20}$ J and we set $k_B = 1$.

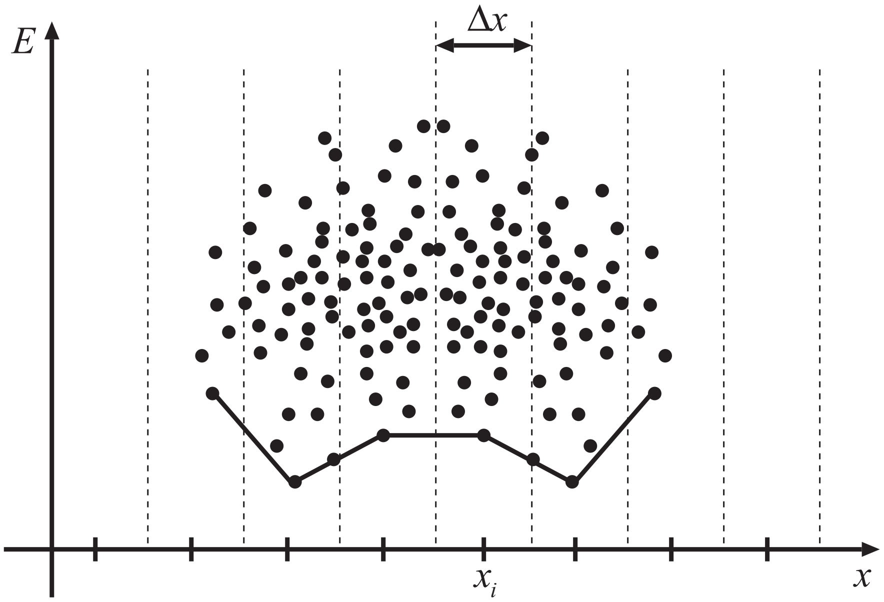

Figure 3.3: The dots illustrate the schematic view of the distribution of states as a function of reaction coordinate x and energy E . Solid line represents the lower energy part of states in a segment. The profile of the lower energy part is essential to determine the FEL especially at low temperature.

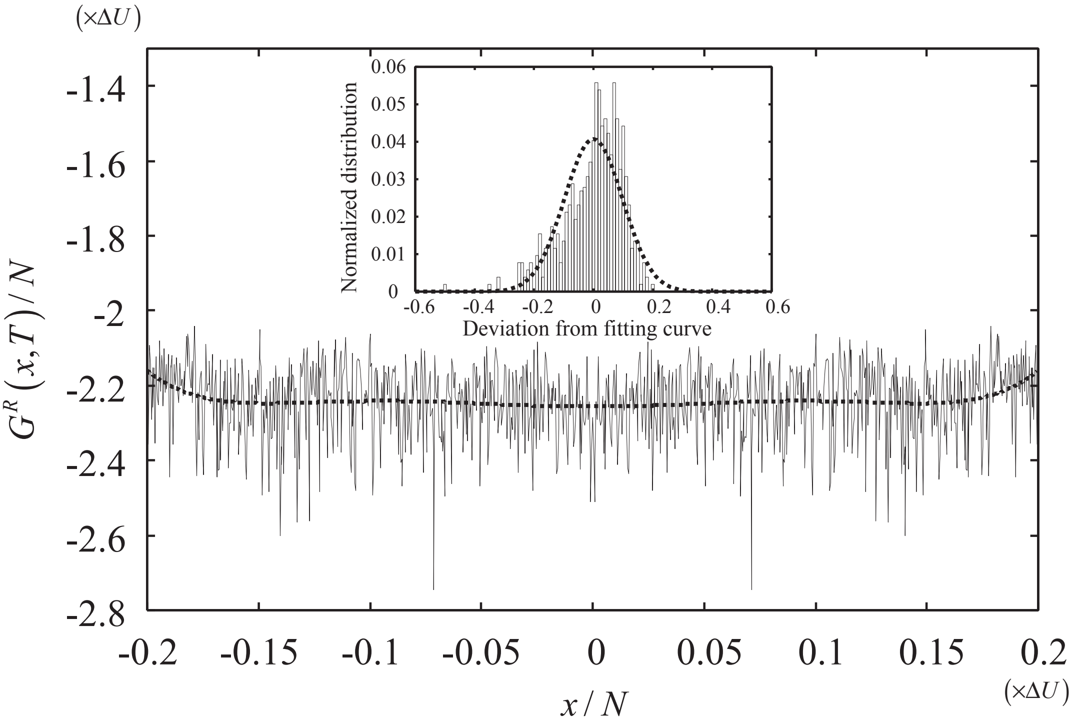

Figure 3.4: The free energy landscape (solid line) and fitted curve (dashed line) of a distorted $3\times3\times3$ lattice model for $T=1$ and $\Delta x=10^{-2}$. The fitting function is $G^R_{fit}(x)=\sum_{k=0}^{3}a_i(x/N)^{2k}$ with parameters $a_6=6731.75$, $a_4=-307$, $a_2=3.9$ and $a_0=-2.26$. The inset of the figure shows the histogram of $\delta G(x_i)$, which is fitted by the normal distribution (dashed line) with the average $\overline{\delta G}=0.0$ and the standard deviation $\sqrt{\overline{\delta G^2}}=0.098$.

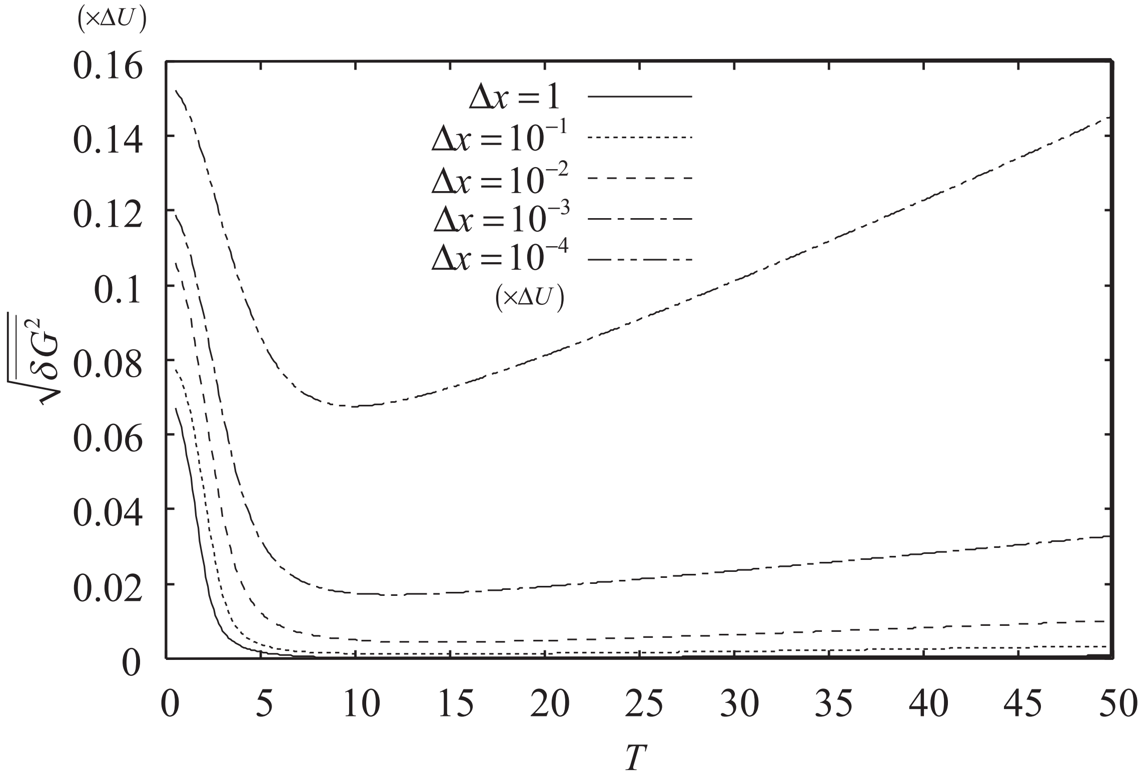

Figure 3.5: The standard deviation $\sqrt{\overline{\delta G^2}}$ for the 26-dipolar-system as the function of the temperature for various segment sizes.

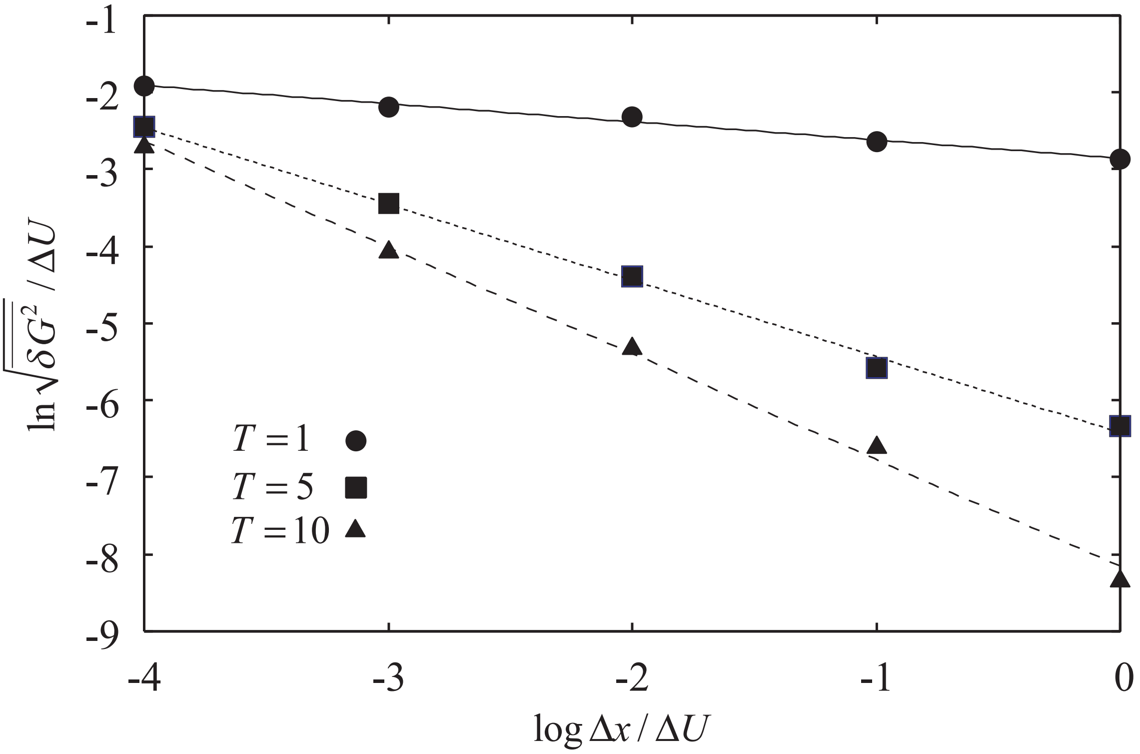

Figure 3.6: The standard deviation $\sqrt{\overline{\delta G^2}}/\Delta U$ for the 26-dipolar-system as the function of the segment size $\Delta x/\Delta U$, where ΔU is the characteristic energy scale of the system. The calculated results can be well fitted by the linear functions in the logarithmic scales.

B. Free Energy Landscapes of a 92-Dipolar-System

Since the number of states is too large to generate for the 92 dipolar system, we sample the states using the Wang-Landau algorithm. We calculate a density of states for the finite segment size Δx and ΔE. In Fig. 3.7, we present the contour plot of the logarithms for density of states $\ln D(x,E)$, for $\Delta x = 10^{-1}$ and $\Delta E = 1$ obtained by the Wang-Landau approach. From the density of states, the free energy landscapes (FELs) are calculated as

$$G^R(x,T) = -k_B T \ln \frac{1}{C} \int_{-\infty}^{\infty} dE \int_{x-\Delta x/2}^{x+\Delta x/2} dx D(x,E) \exp\left(-\frac{E}{k_B T}\right). \tag{3.3.7}$$

Figure 3.8 depicts the calculated FELs of the reactant state $G^R(x,T)/N$ with $\Delta x = 10^{-1}$ for two different temperatures (a) $T = 10$ and (b) $T = 1$. In the same manner as the 26 dipolar system, we estimated the freezing temperature at $T_c \approx 4$. The solid lines in Figs. 3.8(a) and (b) are the calculated results, while the dotted lines represent fitting curves with the parabolic function $G(x) = \alpha + \beta(x/N)^2$ for the range $|x/N| \leq 0.2$. The parameters are chosen to be (a) $\alpha = -7.7$ and $\beta = 5.2$, and (b) $\alpha = -4.6$ and $\beta = 5.1$. Note that the presented results are for the specific set of the positions for dipoles and the quadratic region of the FEL may change slightly depending on the distribution of dipoles.

The calculated FEL for the 92-dipolar-system at high temperature is depicted in Fig. 3.8(a). As discussed in the 26-dipolor-system, the profile of the FEL is governed by the number of states $n(x_i)$ at high temperature. If we assume the energy distribution of states in Gaussian form with the central energy $\overline{E}_i$ and the standard deviation ΔE_i, the free energy is evaluated as

$$\begin{aligned} G^R(x_i,T) &\approx -k_B T \ln \frac{1}{\sqrt{2\pi}\Delta E_i} \int n(x_i) \exp\left(-\frac{\left(E-\overline{E}_i\right)^2}{2\Delta E_i^2}\right) \exp\left(-\frac{E}{k_B T}\right) dE \\ &= -k_B T \ln n(x_i) + \overline{E}_i - \frac{\Delta E_i^2}{2k_B T} \end{aligned}, \tag{3.3.8}$$

where x_i is the ith segment with the region between $x_i - \Delta x/2$ and $x_i + \Delta x/2$.

Near the minimum of free energy surfaces $|x/N| \le 0.2$, since a large number of states are involved in $n(x)$, we can assume Gaussian form for $n(x)$ based on the central limiting theorem. For the high temperature case, the contribution from $-k_B T \ln n(x_i)$ is large and therefore we have the parabolic energy landscapes for $|x/N| \le 0.2$. For large $|x/N|$, however, $n(x)$ contains only a small number of states and deviates from Gaussian due to the failure of the central limiting theorem. (See also Fig. 3.7). Consequently, $G^R(x,E)$ shows parabolic and non-parabolic profiles for small and large $|x/N|$, respectively. We should notice, however, that although such feature exists for any system, the deviation from the parabola may be too small to observe in a real system, since it contains tremendous degrees of freedom that makes the deviation very small.

Figure 3.8(b) shows the FEL for $T=1$. In the low temperature case, FELs are determined by the lower energy part of distribution $D(x, E)$, because the Boltzmann weight in Eq.(3.3.7) suppress the higher energy contributions. Since the lower energy part of $D(x, E)$ is not a smooth function of x as illustrated in Fig. 3.7, the calculated FELs at low temperature exhibit the notched structure as presented in Fig. 3.8 (b). Following the same procedure as the 26-dipolar-system, we have extracted the notched part $\delta G(x)$ for all ranges of x and analyzed their statistics. The amplitude of the notched part of profiles $\sqrt{\overline{\delta G^2}}$ changes depending upon the size of Δx. Due to the limitation of CPU power; however, we can calculate the values of $\sqrt{\overline{\delta G^2}}$ for low temperature $T=1$ only for relatively large segments, i.e. $\Delta x = 0.1$, 0.5 and 1. Thus, by assuming the relation between Δx and $\sqrt{\overline{\delta G^2}}$ found in 3.3.A, here we have extrapolated the value of $\sqrt{\overline{\delta G^2}}$ for small Δx and found $\ln\sqrt{\overline{\delta G^2}}/\Delta U = -0.15\log\Delta x/\Delta U - 2.87$. This relation is in accordance with the change of the total energy and the reaction coordinate by flipping one dipole represented by $\Delta E_{flip}/N$ and Δx_{flip}. In the 92-dipolar-system, we estimate the average solute-solute and solute-solvent interaction energies as $\overline{h} = 0.27$ and $\overline{g} = -0.01$, respectively, and therefore we have $\Delta x_{flip} = 0.02$ and $\Delta E_{flip}/N = 0.06$. From the extrapolated function, we have $\sqrt{\overline{\delta G^2}} = 0.07$ if we regard Δx_{flip} as the segment size. This value is roughly in accordance with $\Delta E_{flip} / N$, which indicates the changes of energy for flipping dipoles are reflecting the amplitude $\sqrt{\overline{\delta G^2}}$.

For a system with large degrees of freedom, the minimal values of Δx can be very small, but, the energy landscape with the segment size $\Delta x \approx \Delta x_{flip}$ is of practical importance for reaction process as mentioned in 3.3.A.

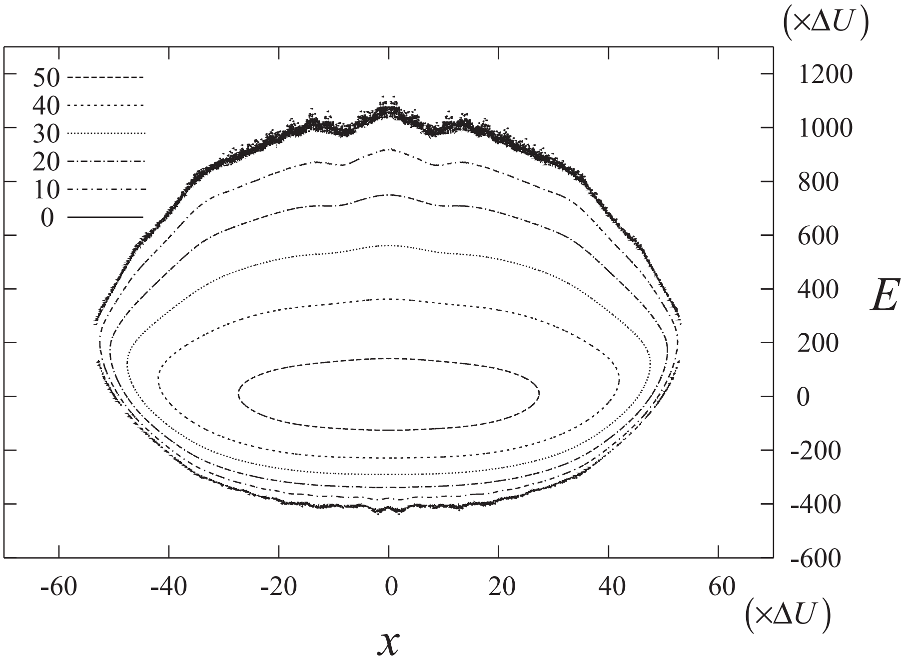

Figure 3.7: The contour plot of the logarithms of the density of states, $\ln D(x, E)$, for the 92-dipolar-system. The segment sizes for the reaction coordinate and energy are chosen to be $\Delta x = 10^{-1}$ and $\Delta E = 1$, respectively. The density of states is obtained by the Wang-Landau approach.

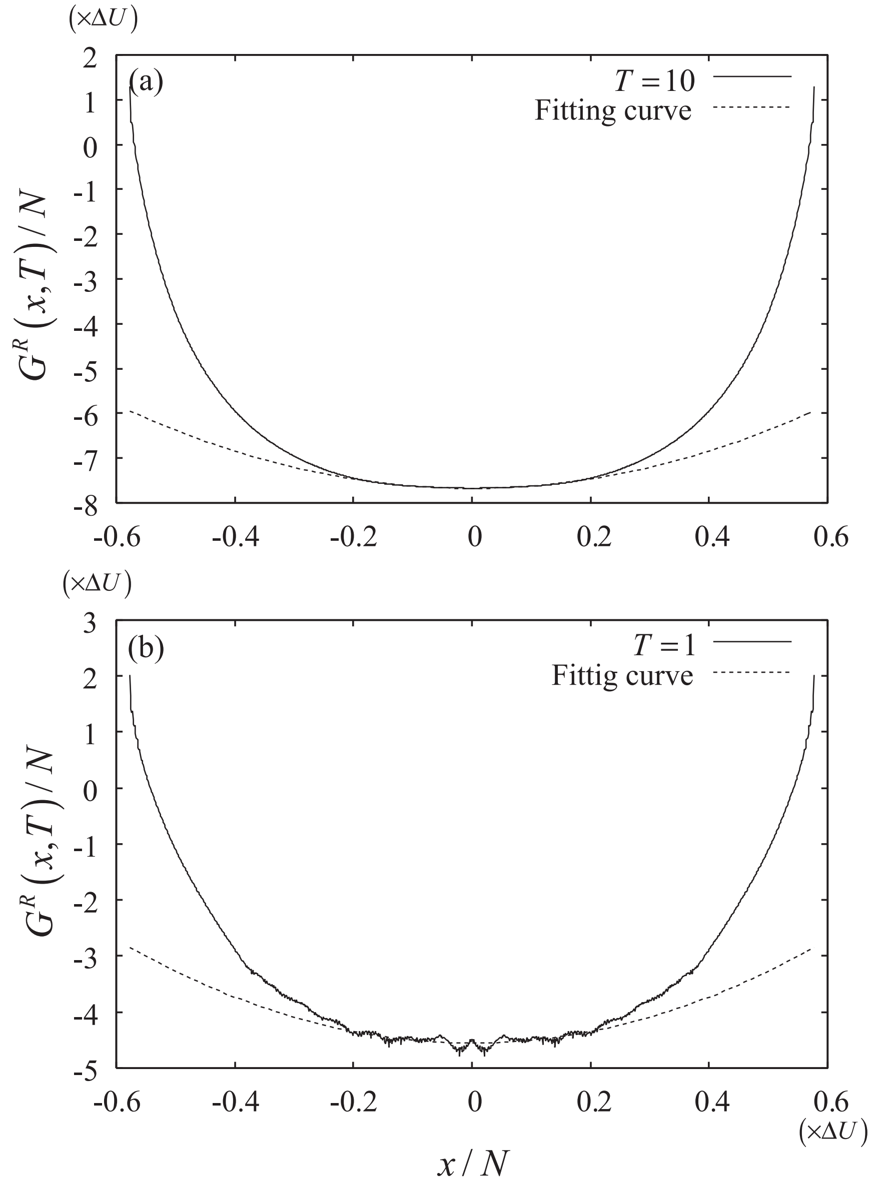

Figure 3.8: The calculated free energy landscapes for the 92 dipolar system $G^R(x,T)/N$ with $\Delta x = 10^{-1}$ for different temperatures (a) $T = 10$ and (b) $T = 1$, respectively.

C. Energy Gap Low for ET Reaction Rates

The FEL for $G^P(x,T)$ is obtained from $G^R(x,T)$ by using Eq. (3.1.4). Using the energy landscapes for the 92-dipolar-system, we calculate the activation energy $\Delta G^{\neq}$ as the function of energy gap ΔG. If we denote the minimum values of the reactant and product states as $G^R_{\min}$ and $G^P_{\min}$, respectively, and express the crossing point of the two surfaces as $x^{\neq}$, we have

$$G^R\left(x^{\neq},T\right)-G^R_{\min}=G^P\left(x^{\neq},T\right)-G^P_{\min}+\Delta G \tag{3.3.9}$$

which allows us to calculate $x^{\neq}$ for fixed ΔG. Since the activation energy $\Delta G^{\neq}$ is given by

$$\Delta G^{\neq}=\left\{G^R\left(x^{\neq},T\right)-G^R_{\min}\right\}, \tag{3.3.10}$$

we can depict the energy gap law by plotting $-\Delta G^{\neq}$ as the function of $-\Delta G$.

Figure 3.9 shows the energy gap dependence of the activation energy at the temperatures $T=10$ (dashed line) and $T=1$ (solid line) calculated from the energy landscapes with the segment size $\Delta x=0.1$, which is slightly larger than Δx_{flip}. All curves of the activation energy are symmetric with respect to the maximum point, since the FEL for the reactant states is the even function. In the low temperature case, $T=1$, the energy gap law exhibits roughness reflected on the notched structure of the energy landscape. Although the profiles of the roughness may change depending upon Δx, the segment size smaller than Δx_{flip} is not necessary to consider the reaction processes because the states can only change through the dipolar flipping in the order of Δx_{flip}. Notice that the microscopic profiles of the roughness differ depending on the distribution of the dipolar positions and if we take an ensemble average for different distributions, such small roughness on the activation energy may not be observed.

Due to the non-parabolic shape of energy landscapes, the energy landscapes are not quadratic besides small $|x|$. The calculated energy gap decreases faster than the quadratic function besides the range about $|\Delta G|\leq 0.2$. This deviation becomes large for high temperature case, since the FEL becomes steep as explained by Eq.(3.3.8).

The energy gap low, Eq. (3.1.1), indicates the maximum reaction rate depends on the reorganization energy λ. When a temperature rises, the profile of activation energy also shifts to the left for $T \geq 10$ as illustrate in Fig. 3.10. For high temperature case, the FEL can be written as $G^R(x,T) \approx -k_B T \ln n(x)$. Since $n(x)$ is approximated by a temperature-independent Gaussian function for small x, we can express the free energy as

$$G^P(x,T) = aT\left(x - \frac{1}{2aT}\right)^2 + G^P_{\min} \tag{3.3.11}$$

where a is some constant and $G^P_{\min}$ satisfies $G^P_{\min} = G^R_{\min} - 1/4aT$. Since the crossing point and the activation energy are expressed as $x^{\neq} = \Delta G + 1/4aT$ and

$$-\Delta G^{\neq} = -\frac{\left((-\Delta G) - \lambda(T)\right)^2}{4\lambda(T)}, \tag{3.3.12}$$

respectively, the peak position of the activation energy is equal to the reorganization energy $\lambda(T) = 1/4aT$. The peak positions of the calculated results are plotted in Fig. 3.10. These results are well fitted by $\lambda(T) = 1/4aT$ with $a = 4.9 \times 10^{-3}$ as illustrated by the solid line in the figure. For studying the solvation saturation effect, Milischuk and Matyushov utilized the relation that the reorganization energy is proportional to $1/T$ for a dipolar solvation system at constant volume.[115] The present results are consistent with their analysis.

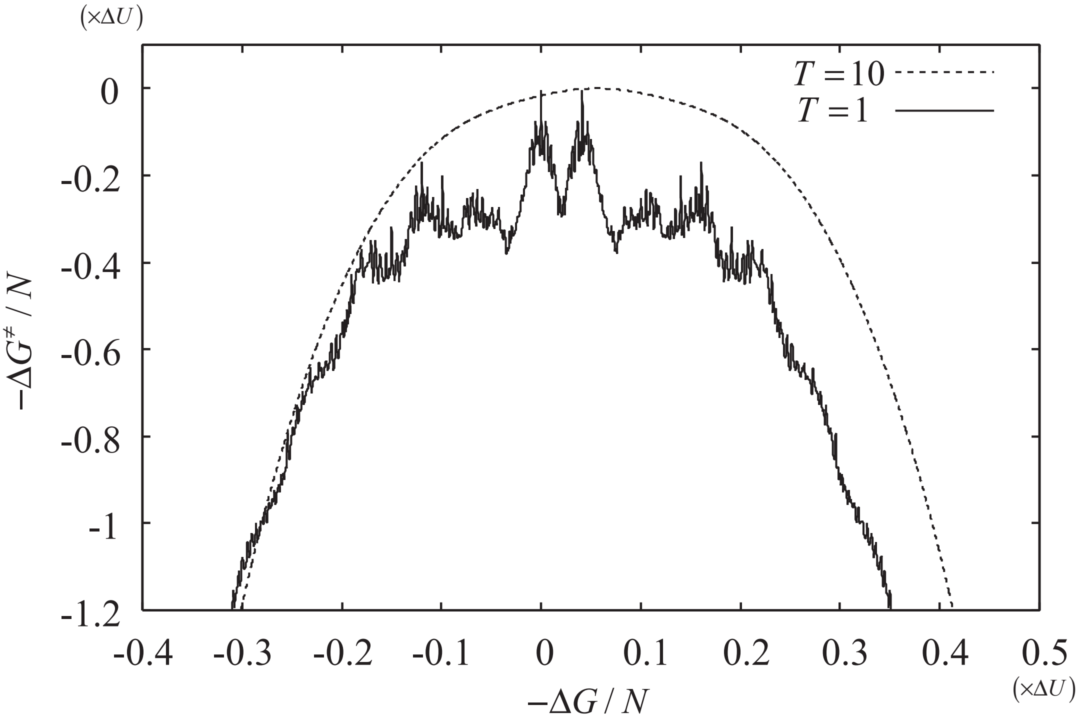

Figure 3.9: The energy gap dependence of the activation energy at the temperatures $T=10$ (dashed line) and $T=1$ (solid line) calculated from the energy landscapes with $\Delta x=0.1$.

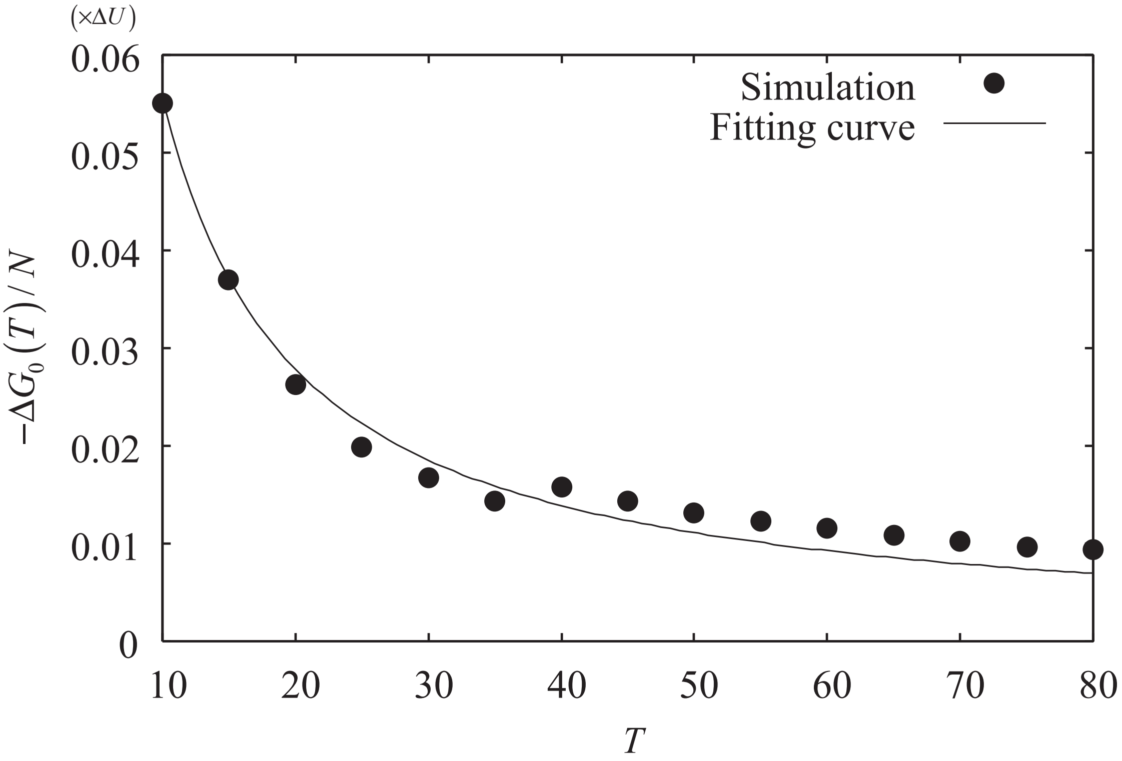

Figure 3.10: The reorganization energy, $\lambda(T)$, which gives the minimum activation energy is plotted for different temperatures for $T \geq 10$ (dots). The solid line represents the fitting curve, $\lambda(T) = 1/4aT$, with $a = 4.9 \times 10^{-3}$.

3.4 Conclusion

We calculated the free energy landscape (FEL) by generating all possible states for a 26-dipolar-system and by using the Wang-Landau sampling algorithm for a 92-dipolar-system. Using the results from the 26-dipolar-system, we analyzed the notched structure of the free energy profiles for different segment sizes of the reaction coordinate Δx. The notched part arose due to the difference in the lowest energy states between the segments. The amplitude, the standard deviation, of the notched part $\sqrt{\delta G^2}$ increased as the segment size decreased especially for low temperatures. The relation between the segment size and the amplitude was in accordance with the relation between the change of reaction coordinate Δx_{flip} and the total energy ΔE_{flip} by flipping a dipole of the system. Although the true free FELs had notched structures whose scale is smaller than Δx_{flip}, a real transition may occur only through the flipping of dipoles. Therefore the scale of Δx smaller than that of Δx_{flip} may not affect on the reaction processes.

Our analysis in the 92-dipolar-system showed that the FEL has a parabolic shape for the small reaction coordinate region at high temperature as the Marcus theory predicted. In the large reaction coordinate region, the profiles exhibited a non-quadratic shape, since the number of states for such segment region was very small and the distribution of states becomes non-Gaussian. At low temperatures, we had estimated the amplitude of the notched part and compared with Δx_{flip} and ΔE_{flip} for the 92-dipolar-system. These values were also in accordance with the relation between Δx and $\sqrt{\delta G^2}$. Although we could not calculate $\sqrt{\delta G^2}$ for very small Δx, we could evaluate $\sqrt{\delta G^2}$ for any Δx with the relation found in the 26-dipolar-system. We should mention that the directions of solvent dipoles used in this model are restricted to pointing toward and opposite to the central solute dipole. This makes a system extremely frustrated and the energy of the solvent dipoles in the equilibrium state becomes much higher than that of a crystal with dipolar orientational relaxation. The FELs below the freezing temperature may be smoother for a realistic system due to the continuity of rotational motion of a solvent dipole.

Finally, the activation energy as the function of the energy gap was calculated by using the FEL for the 92-dipolar-system. At high temperatures, the bell shaped reaction rate was observed. Due to the non-quadratic FEL, the non-quadratic dependency appeared as the energy gap increased. Thus the profile of the calculated reaction rate became steeper than that derived from the quadratic FEL. When the temperature decreased, the parabolic profile of activation energy $\Delta G^{\neq}$ shifted to the lower energy part of ΔG, since the value of the free energy was proportional to the temperature at the high temperature regime. At low temperatures, the profile of the reaction rate became rough due to the notched structure of the FEL. The appearance of roughness is depended on the distributions of dipolar positions and if we take an ensemble average for different distribution of dipoles, this roughness may not be observed. In such case, one should explore dynamical as well as thermal aspects of the system by means of the nonlinear response function to separate inhomogeneous and homogeneous contributions of reaction processes.[116]

Chapter 4

Exploring a Free Energy Landscape by Means of Multidimensional Infrared Spectroscopy

4.1 Introduction

The stable structures of atomic or molecular system under the thermal equilibrium are determined by the contribution of the interaction energy and entropy.[6][7][8] The free energy landscape (FEL) is the effective potential which contains both effects and is wildly used in several research fields. In glass and amorphous solid, inhomogeneous structure of molecules accompanied by the quenching temperature [1][117] and the native structure of proteins[118][119] are discussed in terms of the FEL. In addition to understanding the stable structure of the systems, the FEL is of fundamental importance to understand the inverted parabolic or bell shaped dependence of the electron transfer (ET) rate.[3][4]

As mentioned in the Chapter 1, the FEL has been used in the framework for the time-dependent-Ginzburg-Landau (TDGL) approach to investigate dynamical phenomena of superconductors [11], domain walls and interfaces.[12][13] However there is a possibility that the dynamical behavior is an independent issue for the FEL, since the FEL is defined under the thermal equilibrium. In addition the FEL is highly conceptual quantity because it is not direct observable. A final goal of our research is to relate the structure of the FEL to the system dynamics on the FEL.

We have employed a simple model representing a dipolar crystal system to reduce the degrees of freedom as was done for protein [44] and solvated ion system.[25][57][61][64] We consider the system consists of dipoles[120][121] and employ this model to calculate the FEL at various temperatures by generating all possible states. We depict the FEL as the function of total dipole moments (polarization), which is the macroscopic observable of the system. We monitor the dynamics not only by linear absorption spectroscopy, but also by multidimensional spectroscopy. The sensitivity of two-dimensional (2D) spectroscopy is utilized to characterize the dynamics on different FELs. Here, we calculate two-dimensional signals corresponding to infrared (IR) and far IR defined by the four-body correlation functions of dipole operators.

The outline of this chapter is as follows. In the next section we briefly explain our simulation model and procedure to calculate the FEL. In section 4.3, we set up the master equations for the present model corresponding to the single flip and single-double mixed flips dynamics. The procedures to calculate linear absorption and third-order 2D signals are also explained. We present the calculated FEL in Sec. 4.4. The 1D and 2D signals calculated from the microscopic master equation approach and their analysis are given in Sec. 4.5. We compare our microscopic results with the signals calculated from the phenomenological Smoluchowski equation approach in Sec. 4.6. We close with our conclusions in Sec. 4.7.

4.2 Simulation Model

We start by assuming regular and distorted two-dimensional lattice models for dipolar molecules, which is an extension of our formally used models developed to analyze the energy landscape.[25][26] The position of each dipole is given by $\mathbf{r}_j = \mathbf{a}_j + \delta\mathbf{a}_j$ where $\mathbf{a}_j$ is the j th lattice point vector and $\delta\mathbf{a}_j$ is the random displacement from lattice point. The j th dipole is described by the angle θ_j and the fixed dipole strength μ; that dipole moment is then expressed as $\mu\mathbf{S}_j\left(\theta_j\right)$, where $\mathbf{S}_j\left(\theta_j\right) = \left(\cos\theta_j, \sin\theta_j\right)$ is the unit vector of the dipole moment. All dipoles interact through the dipole-dipole interaction expressed in the set of angels $\boldsymbol{\theta} = \left\{\theta_j\right\}$ as

$$E\left(\boldsymbol{\theta}\right) = \mu^2 \sum_{j=2}^{N} \sum_{k=1}^{j-1} h_{jk}\left(\theta_j, \theta_k\right), \tag{4.2.1}$$

where

$$h_{jk}\left(\theta_j, \theta_k\right) = \frac{\mathbf{S}_j(\theta_j)\cdot\mathbf{S}_k(\theta_k)\left|\mathbf{r}_{jk}\right|^2 - 3\left(\mathbf{S}_j(\theta_j)\cdot\mathbf{r}_{jk}\right)\left(\mathbf{S}_k(\theta_k)\cdot\mathbf{r}_{jk}\right)}{\left|\mathbf{r}_{jk}\right|^5} \tag{4.2.2}$$

with $\mathbf{r}_{jk} = \mathbf{r}_j - \mathbf{r}_k$ and N is the total number of dipoles. Although this model is intensely simplified, it still contains enormous degrees of freedom and is impossible to evaluate the FEL. Since we are interested in a motion of the system at low temperature, we may reduce the degrees of freedom by choosing a small subset of states near the lowest energy configuration. We thus construct a further simplified model with the following two steps. We first restrict each dipole to point only four directions $\theta_j = (2n-1)\pi/4$ ($n = 1 \sim 4$) and find the energy minimum configuration denoted by $\boldsymbol{\theta}^0 = \left\{\theta_j^0\right\}$ by generating all configurations of $\boldsymbol{\theta}$ (dotted arrows in Fig. 4.1). Using this minimum configuration, we then construct a two-state dipolar model by adding the two values of the angular shifts $\delta\theta_j = \pm\pi/8$ to each θ_j^0 as depicted by the solid arrows in Fig. 4.1. This model simulates the librational fluctuations around the energy minimum. We set $\delta\theta_j = \pm\pi/8$ to have a discredited expression of a macroscopic variable (i.e., an order parameter or a reaction coordinate) for the FEL. This model may be oversimplified to study a real system, but it should be sufficient to grasp a relation between the FEL and dynamics.

From Eqs. (4.2.1) and (4.2.2), the total energy of our model is written as $E\left(\boldsymbol{\theta}^0 + \delta\boldsymbol{\theta}\right)$, where the set of angular shifts is defined by $\delta\boldsymbol{\theta} = \left\{\delta\theta_j\right\}$. We set $\mu = 1.85$ and $L = 1$ in the units of Debye and $2.1\mathring{\mathrm{A}}$, respectively, as the typical of dipolar liquid. The characteristic energy is then evaluated as $\Delta U = 1.08\times10^{-20}\,\mathrm{J}$, which is about $2.5\left(k_B T\right)$ at room temperature. The displacements from the lattice points obey a Gaussian distribution with average $\left\langle \delta\mathbf{a}_j \right\rangle = 0$ and standard deviation $\left\langle \delta\mathbf{a}_j^2 \right\rangle$. We chose two parameters for 4×4 lattice corresponding to the structural disorder case $\left\langle \delta\mathbf{a}_j^2 \right\rangle = 0.1$ and the regular lattice case $\left\langle \delta\mathbf{a}_j^2 \right\rangle = 0$. We utilize the open boundary condition to avoid undesired effects that arise from a treatment of boundary.

To study FEL by means of experiments, we depict the FEL as the function of an experimental observable. Here, the reaction coordinate or the order parameter is chosen to be the total polarization defined by

$$P = \sum_{j=1}^{N} \mu_j^y = \mu \sum_{j=1}^{N} \sin\left(\theta_j^0 + \delta\theta_j\right), \tag{4.2.3}$$

where μ_j^y is the jth dipole moment for the vertical direction. Since θ_j^0 can take only $\theta_j = (2n-1)\pi/4$ and we chose $\delta\theta_j = \pm\pi/8$, P takes discrete $N+1$ values for N dipolar system with the constant step size $\Delta P = \sqrt{2}\mu\sin\left(\pi/8\right)$. If N_+ $\left(N_-\right)$ is the number of dipoles whose θ_j^0 satisfies $0 \le \theta_j^0 < \pi$ $\left(\pi \le \theta_j^0 < 2\pi\right)$, the minimum and maximum values of the reaction coordinate become $P_{\min} = \mu\left(\sin\left(\pi/8\right)N_+ - \sin\left(3\pi/8\right)N_-\right)$ and $P_{\max} = \mu\left(\sin\left(3\pi/8\right)N_+ - \sin\left(\pi/8\right)N_-\right)$, respectively. For our model, N_+ and N_- satisfy $N_+ = N_- = N/2$ because the systems are symmetric with the exclusion of the small deviated positions of dipoles. The values of P is expressed by introducing an integer k which meets $-N/2 \le k \le N/2$ in a symmetric form as

$$P\left(k\right) = k\sqrt{2}\mu\sin\left(\frac{\pi}{8}\right). \tag{4.2.4}$$

The FEL is then given by

$$F\left(P(k)\right) = -k_B T \ln \sum_{i=1}^{2^N} \delta_{P(k),\,P_i} \exp\left(-\frac{E_i}{k_B T}\right) \tag{4.2.5}$$

where P_i and E_i are the polarization and energy for the ith state, respectively, and $\delta_{a,b}$ is the Kronecker's delta. We denote the polarization for the ith state by P_i and the reaction coordinate specified by an integer k by $P\left(k\right)$.

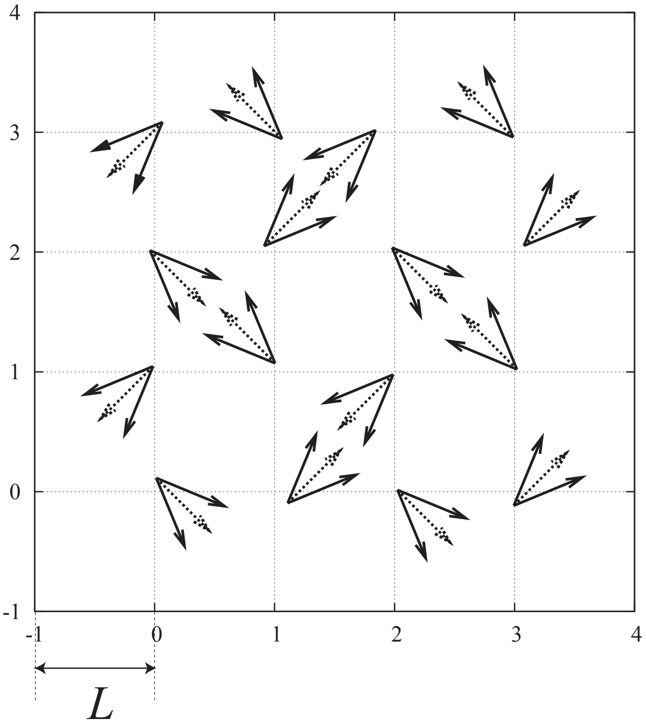

Figure 4.1: The Schematic view of a model for representing dipolar molecules. Dipoles are located on the distorted lattice sites and interact through the dipole-dipole interactions. Each dipole is allowed to point two directions (solid arrows) to represents the librational fluctuations. The dotted arrows represent the centers of librational motions, which are obtained from the energy minimum of the four states dipoles model.

4.3 Dynamics and Observable of Dipolar System

A. Master Equations for Single and Single-Double Flips Dynamics

First we should point out that our system is not kinetic, since our Hamiltonian is specified by the configurations of the discretized dipoles and does not have a kinetic term. To yield the time-evolution, we assume a stochastic dynamics among the dipole states that brings the system to be in the thermal equilibrium state at $t \to \infty$. We do not use kinetic Monte Carlo (MC) approach introduced by Glauber [43], since we must study dynamics at very low temperature, where the MC sampling does not work properly. Taking an advantage of a small system, we use the master equation approach for all 2^N dipolar states. Since the master equation employs a probability distribution function and does not rely on the sampling procedure, we can numerically calculate the time-evolution of the system at the same CPU at any temperatures. We ordered 2^N states as $E_1 < E_2 < \cdots < E_{2^N}$, where E_k is the interaction energy evaluated from Eq.(4.2.1) for the *k*th lowest energy state $\boldsymbol{\theta}^0 + \delta\boldsymbol{\theta}_k$. The polarization of $\delta\boldsymbol{\theta}_k$ is evaluated from Eq.(4.2.3) and is expressed as P_k. We denote the probability distribution for all states by vector $\vec{\rho}(t) = \left[\rho_1(t), \rho_2(t), \cdots \rho_{2^N}(t)\right]^t$. This master equation is a rate equation for the probability distributions and is expressed as

$$\frac{\partial}{\partial t}\vec{\rho}(t) = -\mathbf{L}\vec{\rho}(t), \tag{4.3.1}$$

where $-\mathbf{L}$ is the transition matrix whose element $(-\mathbf{L})_{kl}$ describes the transition probability between the *l*th and *k*th states. We introduce the polarization vector given by $\vec{P} = \sum_k P(k)\vec{D}_{P(k)}$, where

$$\vec{D}_{P(k)} = \left[\delta_{P(k),P_1}, \delta_{P(k),P_2}, \delta_{P(k),P_3}, \cdots, \delta_{P(k),P_{2^N}}\right]^t. \tag{4.3.2}$$

The operator $\vec{D}_{P(k)}$ allows us to calculate the probability to have the polarization $P(k)$ from the probability distribution function $\vec{\rho}(t)$. The total polarization is then expressed as

$$P(t) = \vec{P} \cdot \vec{\rho}(t), \tag{4.3.3}$$

where the dot represents the inner product.

As was mentioned in Chapter 1, the FEL may be the same for the same system with different dynamics. To illustrate this point, we consider two cases of $-\mathbf{L}$ that can be specified by the connectivity coefficient of dipolar states. Consider the qth lowest energy state $\delta\boldsymbol{\theta}_q$. Suppose if we flip a dipole and energy becomes E_p, the connectivity coefficients are specified as $C^{(1)}_{p,q}=1$. Letting be unreachable p'th states from qth state with a single dipole flipping, the coefficients satisfy $C^{(1)}_{p',q}=0$ for the single flip case. If the state is in the qth lowest energy state $\delta\boldsymbol{\theta}_q$ and if the energy becomes E_p with a two-dipolar flipping, we set $C^{(2)}_{p,q}=1$ and $C^{(2)}_{p',q}=0$ for unreachable p'th state for the double flip case. The connectivity coefficients for n flipping of dipoles $C^{(n)}_{p,q}$ can also be defined accordingly. In Monte Carlo approach, n=1 corresponds the single flip sampling per one MC step yielding the Glauber dynamics, whereas n=2 corresponds to the double flip sampling. Since $-\mathbf{L}$ has to satisfy the detailed balance condition, transition matrixes for n flipping dynamics have to be in the form of

$$(-\mathbf{L}^{(n)})_{i,j}=\begin{cases} C^{(n)}_{i,j}\exp\left(-\Delta\tilde{E}_{i,j}/k_BT\right) & \text{for } \tilde{E}_i>\tilde{E}_j \\ C^{(n)}_{i,j} & \text{for } \tilde{E}_i<\tilde{E}_j \end{cases}, \tag{4.3.4}$$

where $\Delta\tilde{E}_{i,j}$ is the energy difference between i th and j th states, i.e. $\Delta\tilde{E}_{i,j}=\tilde{E}_i-\tilde{E}_j$. Here, we consider the linear combination of n=1 and 2 flippings defined by

$$-\mathbf{L}=-\alpha\mathbf{L}^{(1)}-\beta\mathbf{L}^{(2)} \tag{4.3.5}$$

to discuss the different dynamics by a choice of the constants α and β.

B. Laser-System Interactions

To calculate response functions, we need to implement an external perturbation based on physical considerations, since our model is not kinetic system. When we apply an external field B to the system, the total energy of the system increases as $-P_jB$ for the j th state. If B is small enough, we can expand the transition matrix for the total Hamiltonian in terms of B. For the single flip case n=1, this is written as

$$\frac{\partial}{\partial t}\vec{\rho}(t)=\left(-\mathbf{L}^{(1)}+B\boldsymbol{\mu}\right)\vec{\rho}(t), \tag{4.3.6}$$

where $-\boldsymbol{\mu}$ is the dipolar interaction whose elements are given by

$$\boldsymbol{\mu}_{i,j}=\begin{cases}(-\mathbf{L}^{(1)})_{i,j}\Delta P_{i,j}/k_BT & \text{for } i>j\\ 0 & \text{for } i<j\end{cases} \tag{4.3.7}$$

with $\Delta P_{i,j}=P_i-P_j$. As discussed for $-\mathbf{L}$, we may define the excitation for any flipping number n. As we need to excite the system in the same manner to study the effects of different time-evolution, we consider the single flip excitation case only.

C. First- and Third-Order Response Functions

The optical observable of the system is expressed as the response functions of dipole moment or polarization.[81] For the first-order linear and third-order two-dimensional (2D) infrared, far infrared and THz spectroscopies, the signals are expressed in terms of a dipole operator $\hat{\mu}$ as $S(t_1)=i\,tr\left\{\hat{\mu}\hat{G}(t_1)\left(\hat{\mu}^{\times}\hat{\rho}_{eq}\right)\right\}/\hbar$ and $S(t_3,0,t_1)=i^3tr\left\{\hat{\mu}\hat{G}(t_3)\hat{\mu}^{\times}\left[\hat{\mu}^{\times}\hat{G}(t_1)\left(\hat{\mu}^{\times}\hat{\rho}_{eq}\right)\right]\right\}/\hbar^3$ [86], where $\hat{\rho}_{eq}$ is the equilibrium distribution and we define $i\hat{A}^{\times}\hat{B}/\hbar\equiv i[\hat{A},\hat{B}]/\hbar$ in the quantal case or $i\hat{A}^{\times}\hat{B}/\hbar\equiv\{\hat{A},\hat{B}\}$ in the classical case.[122] By using the quantal or classical Liouville operator of the system $\hat{L}$, the time-evolution operator is expressed as $\hat{G}(t)\hat{A}\equiv \mathrm{e}^{-Lt}\hat{A}$. For the master equation, the response functions are expressed as

$$S(t_1)=\sum_k P(k)H_{\boldsymbol{\mu}}\left(P(k),t_1\right), \tag{4.3.8}$$

and

$$S(t_3,0,t_1)=\sum_k P(k)H_{\boldsymbol{\mu\mu\mu}}\left(P(k),t_3,0,t_1\right), \tag{4.3.9}$$

where

$$H_{\boldsymbol{\mu}}\left(P(k),t_1\right)=\vec{D}_{P(k)}\exp\left[-\mathbf{L}t_1\right]\boldsymbol{\mu}\vec{\rho}_{eq}, \tag{4.3.10}$$

and

$$H_{\boldsymbol{\mu\mu\mu}}\left(P(k),t_3,0,t_1\right)=\vec{D}_{P(k)}\cdot\exp\left[-\mathbf{L}t_3\right]\boldsymbol{\mu\mu}\exp\left[-\mathbf{L}t_1\right]\boldsymbol{\mu}\vec{\rho}_{eq}. \qquad (4.3.11)$$

The vector $\vec{\rho}_{eq}$ represents the thermal equilibrium distribution whose component is defined by

$$\left(\vec{\rho}_{eq}\right)_i=\exp\left(-E_i/k_BT\right)/Z, \qquad (4.3.12)$$

in which Z is the partition function. Analogues to a quantal case, the right-hand side of Eqs.(4.3.10) and (4.3.11) can be read from the right to left as follows. The total system is initially in the equilibrium state $\vec{\rho}_{eq}$. The initial state is then modified by the first laser pulses via the dipole operator as $\boldsymbol{\mu}$ at $t=0$ and is propagated for time t_1 by $\exp\left[-\mathbf{L}t_1\right]$. The probability distribution functions is now given by $\exp\left[-\mathbf{L}t_1\right]\boldsymbol{\mu}\vec{\rho}_{eq}$. The linear absorption (1D) signal is the expectation value of polarization given by $\sum_k P(k)H_{\boldsymbol{\mu}}\left(P(k),t_1\right)$. In the third-order 2D measurements, after the first excitation and time evolution for t_1, the system is further excited by the second and third dipole interactions expressed as $\boldsymbol{\mu\mu}$. After these excitations, the system is propagated for the time period t_3 by $\exp\left[-\mathbf{L}t_3\right]$ as $\exp\left[-\mathbf{L}t_3\right]\boldsymbol{\mu\mu}\exp\left[-\mathbf{L}t_1\right]\boldsymbol{\mu}\vec{\rho}_{eq}$ and, finally, the expectation value of the dipole moment at t_1+t_3 is obtained by $\sum_k P(k)H_{\boldsymbol{\mu\mu\mu}}\left(P(k),t_3,0,t_1\right)$. Using the above procedure, we can calculate 1D and 2D signals from master equation approach.

4.4 Free Energy Landscapes

In Fig. 4.2, we illustrate the free energy landscapes (FELs) in the case of 4×4 distorted and regular lattice at various temperatures: (a) $T=10$, $\left\langle\delta\mathbf{a}_j^2\right\rangle=0.1$; (b) $T=1$, $\left\langle\delta\mathbf{a}_j^2\right\rangle=0.1$; (c) $T=0.1$ $\left\langle\delta\mathbf{a}_j^2\right\rangle=0.1$; (d) $T=10$, $\left\langle\delta\mathbf{a}_j^2\right\rangle=0$; (e) $T=1$, $\left\langle\delta\mathbf{a}_j^2\right\rangle=0$; and (f) $T=0.1$, $\left\langle\delta\mathbf{a}_j^2\right\rangle=0$. Here and after, we set $k_B=1$. We analyze the temperature dependence of the heat capacity and find a sharp peak $T_c\approx1$ that are corresponded to the freezing temperature of dipolar librational motions. Therefore the cases for (c) and (f) are in the glassy state. These landscapes are directly calculated from Eq. (4.2.5) by generating all possible dipolar states numerically.

To elucidate a profile for each of FELs, we introduce the density of states as the function of $P(k)$, and E expressed as

$$n\left(P(k),E\right)dE=\Omega\left(P(k)\right)g\left(P(k),E\right)dE \tag{4.4.1}$$

where $g\left(P(k),E\right)$ is the distribution of the density of state between E and $E+dE$ for fixed $P(k)$ and $\Omega\left(P(k)\right)$ is the total number of states for $P(k)$ defined by

$$\Omega\left(P(k)\right)=\sum_{r=|k|}^{N/2}{}_{N/2}C_r\,{}_{N/2}C_{r-|k|}=\frac{N!}{\left(N/2+|k|\right)!\left(N/2-|k|\right)!}. \tag{4.4.2}$$

From Eq. (4.4.1), the FEL given by Eq. (4.2.5) is evaluated as

$$F\left(P(k)\right)=-k_BT\ln\int dEg\left(P(k),E\right)\exp\left(-E/k_BT\right)-TS^*\left(P(k)\right), \tag{4.4.3}$$

where $S^*\left(P(k)\right)=k_B\ln\Omega\left(P(k)\right)$ is the configuration entropy given by

$$S^*\left(P(k)\right)\simeq -k_BN\left[\left(\frac{1}{2}+\frac{|k|}{N}\right)\ln\left(\frac{1}{2}+\frac{|k|}{N}\right)+\left(\frac{1}{2}-\frac{|k|}{N}\right)\ln\left(\frac{1}{2}-\frac{|k|}{N}\right)\right]. \tag{4.4.4}$$

If we assume the energy distribution $g\left(P(k),E\right)$ obeys Gaussian form with the central energy $\bar{E}\left(P(k)\right)$ and the standard deviation $\Delta E\left(P(k)\right)$, Eq. (4.4.3) is evaluated as

$$F\left(P(k)\right)=\bar{E}\left(P(k)\right)-\frac{\Delta E^2\left(P(k)\right)}{2k_BT}-TS^*\left(P(k)\right). \tag{4.4.5}$$

The profile of the FEL is governed by the configuration entropy $S^*\left(P(k)\right)$ at high temperature. By expanding $F\left(P(k)\right)\approx -TS^*\left(P(k)\right)$ in power of $\left|P(k)\right|$ up to the fourth order, we have

$$\frac{F(P)}{N}\approx -k_BT\left[\ln 2-\frac{2}{\Delta P^2}\left(\frac{P}{N}\right)^2-\frac{4}{3\Delta P^4}\left(\frac{P}{N}\right)^4\right] \tag{4.4.6}$$

where $\Delta P=\sqrt{2}\mu\sin\left(\pi/8\right)$. Analogues to the electron transfer case [26], this result indicates that the profile of the FELs is parabolic for the small P, while an additional quartic contribution to the FELs is found for the large P. Since the quartic term arises from $TS^*\left(P(k)\right)$, this contribution is attributed to the entorpic origin. In the case of Figs. 4.2(a) and 4.2(d), the FEL is looks parabolic in the small region of P.

When the temperature drops, the simulated FELs are no longer smooth and a remarkable difference appears between the distorted case (Fig. 4.2(c)) and the regular case (Fig. 4.2(f)). This feature can be explained from the distribution of states as a function of the polarization P and the energy E as illustrated in Fig. 4.3. For the regular case, the states are highly degenerated (the close circles in Fig. 4.3) due to the symmetry of the system, while for the distorted case, the states are not degenerated and irregularly distributed (the open circles in Fig. 4.3) because of the frustrated interactions among the dipoles. Since the FELs are determined by the lowest energy states at very low temperature due the Boltzmann factor in Eq. (4.2.5), the FEL of the distorted lattice exhibits prominent irregular profiles.

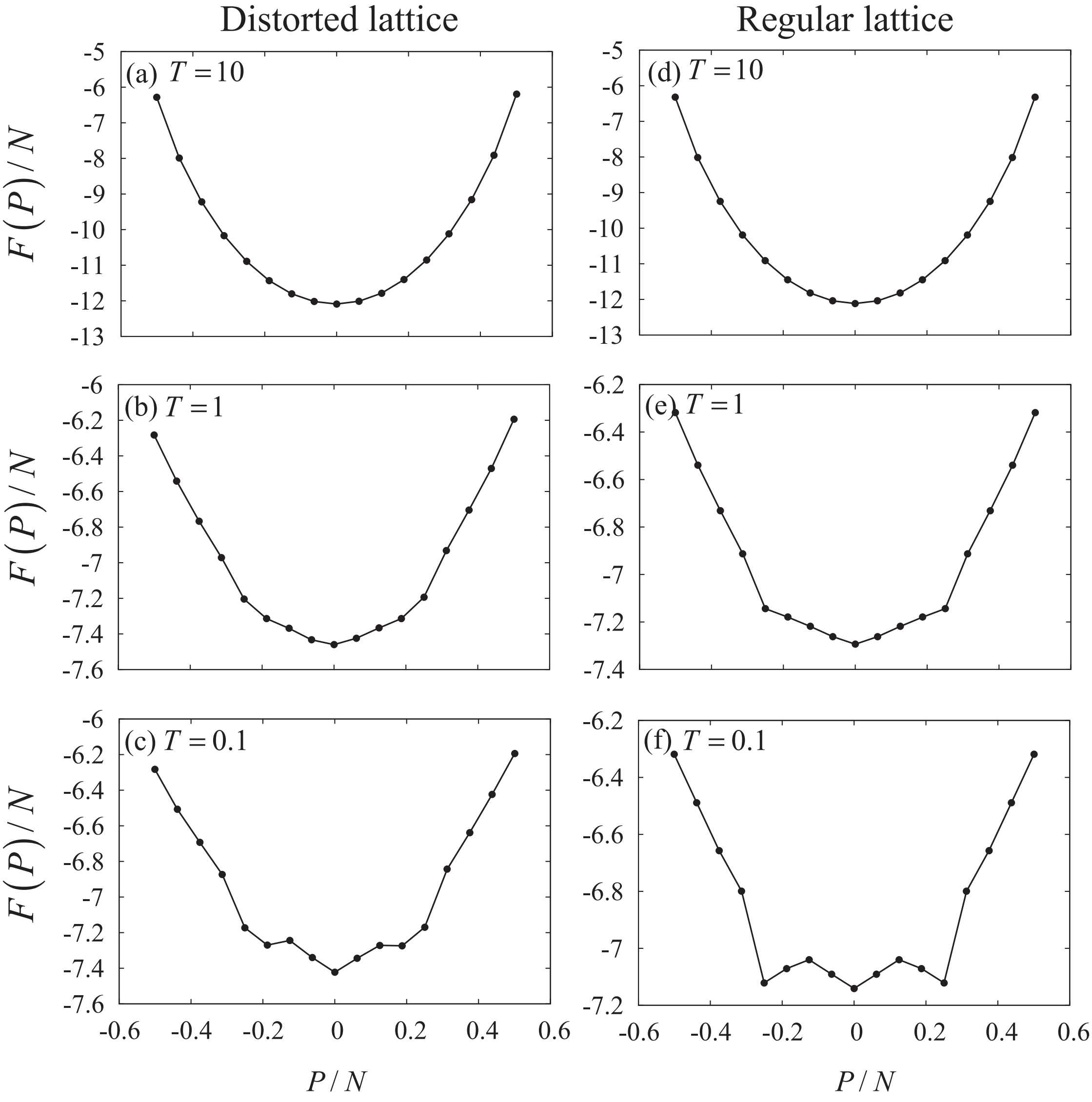

Figure 4.2: The FELs as the function of the polarization P in the case of 4×4 distorted and regular lattices at various temperatures: (a) $T=10$, $\left\langle \delta\mathbf{a}_j^2 \right\rangle = 0.1$; (b) $T=1$, $\left\langle \delta\mathbf{a}_j^2 \right\rangle = 0.1$; (c) $T=0.1$ $\left\langle \delta\mathbf{a}_j^2 \right\rangle = 0.1$; (d) $T=10$, $\left\langle \delta\mathbf{a}_j^2 \right\rangle = 0$; (e) $T=1$, $\left\langle \delta\mathbf{a}_j^2 \right\rangle = 0$; and (f) $T=0.1$, $\left\langle \delta\mathbf{a}_j^2 \right\rangle = 0$.

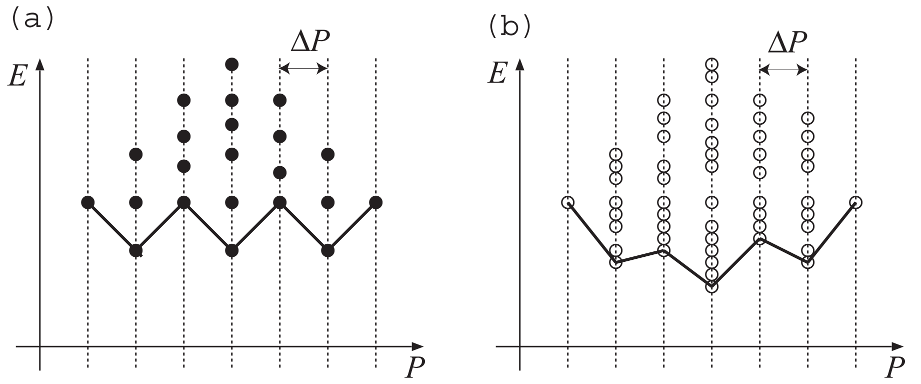

Figure 4.3: The schematic pictures of the distribution of states as a function of the polarization P and energy E. The solid line represents FELs for (a) a regular lattice case and (b) a distorted lattice case. The states are highly degenerated due to the symmetry of the system shown as the close circle, while the states are degenerated and irregularly distributed shown as the open circle in (b). As a result, the FEL for the distorted case exhibits prominent irregular profiles.

4.5 Optical Responses

A. One-Dimensional Signals

Following the procedures explained in Sec. 4.3.C, we have calculated the first- and third-order response functions and plotted them as the signals in one- and two-dimensional spectroscopies. In Figs. 4.4 (a)-(f) , the linear absorption (1D) signal $S\left(t_1\right)$ for (i) the single-flip case, $\alpha = 1$ and $\beta = 0$ (solid line), and (ii) the single-double mixed flips case, $\alpha = 0.5$ and $\beta = 1$ (dashed line), are plotted for the same sets of parameters $\left\langle \delta \mathbf{a}_j^2 \right\rangle$ and T used in Figs. 4.2 (a)-(f). Although the relaxation rates are different in each case, we find that solid and dashed lines in Figs. 4.4(a) and 4.4(d) at the high temperature case are well fitted by a single exponential function, whereas the solid and dashed lines in Figs. 4.4(b) and 4.4(e) are fitted by the sum of exponential functions at the intermediate temperature. At the low temperature, the solid lines are single exponential function, while the dashed lines are represented by the sum of exponential functions in Figs. 4.4(c) and 4.4(f).

To investigate these features, we consider a relaxation mode analysis, which utilizes the eigenvalues and eigenmodes of the master equation for a system with complex interactions.[123][124] In this analysis, the time-relaxation of a two-body correlation function is characterized by a sum of exponential functions with their decay rates defined by the eigenvalues of the master equation. If the number of the eigenmodes involved in the system is enormous and the eigenvalues are well distributed in the energy space due to the complex interactions in the system, the signal decays non-exponentially as shown in the case of a two-dimensional $\pm$ Ising model at the critical point. Despite the complexity of the interactions between the dipoles, present results decay more or less exponentially regardless of the temperatures. This is because the excitation induced by laser pulses is highly symmetrical against to P and therefore the laser interaction excites only a few modes which decay exponentially.

To see this point more closely, we depict $H_{\boldsymbol{\mu}}\left(P, t_1\right)$ given in Eq.(4.3.10) which represents the deviation of the distribution from the equilibrium state after the laser interaction $\boldsymbol{\mu}$ at time $t = 0$ for given P. Figures 4.5 (a)-(f) illustrate the change of

$H_{\mu}(P,t_1)$ in time for distorted cases and regular lattice cases at different temperatures for the single flip dynamics in the same order of Figs. 4.4 (a)-(f). In each figure, the line above the P axis shows the corresponding FEL. Here, we plot the single flip case only, since the profiles of $H_{\mu}(P,t_1)$ for different temperatures and configurations in the single flip and single-double flips cases are approximately analogues, if we normalized the time scale of each figures by their relaxation rates estimated from Fig. 4.4. As all figures in Fig. 4.5 indicate, the primary cause of the signal relaxation is not from the movement of $H_{\mu}(P,t_1)$ toward the $P=0$ point but from the decrease of $H_{\mu}(P,t_1)$ for the fixed position of P. Since $H_{\mu}(P,t_1)$ decays monotonically with keeping their profiles at the high temperature and very low temperature as shown in Figs. 4.5 (a) and (d) and Figs. (c) and (f), respectively, we may conclude that the excited states are composed of either the single eigenmode or the eigenmodes that have similar eigenvalues. At the intermediate temperature in Figs. 4.5(b) and 4.5(e), the profile of $H_{\mu}(P,t_1)$ slightly change as time goes indicating those excite states are composed of the eigenmodes with different eigenvalues.

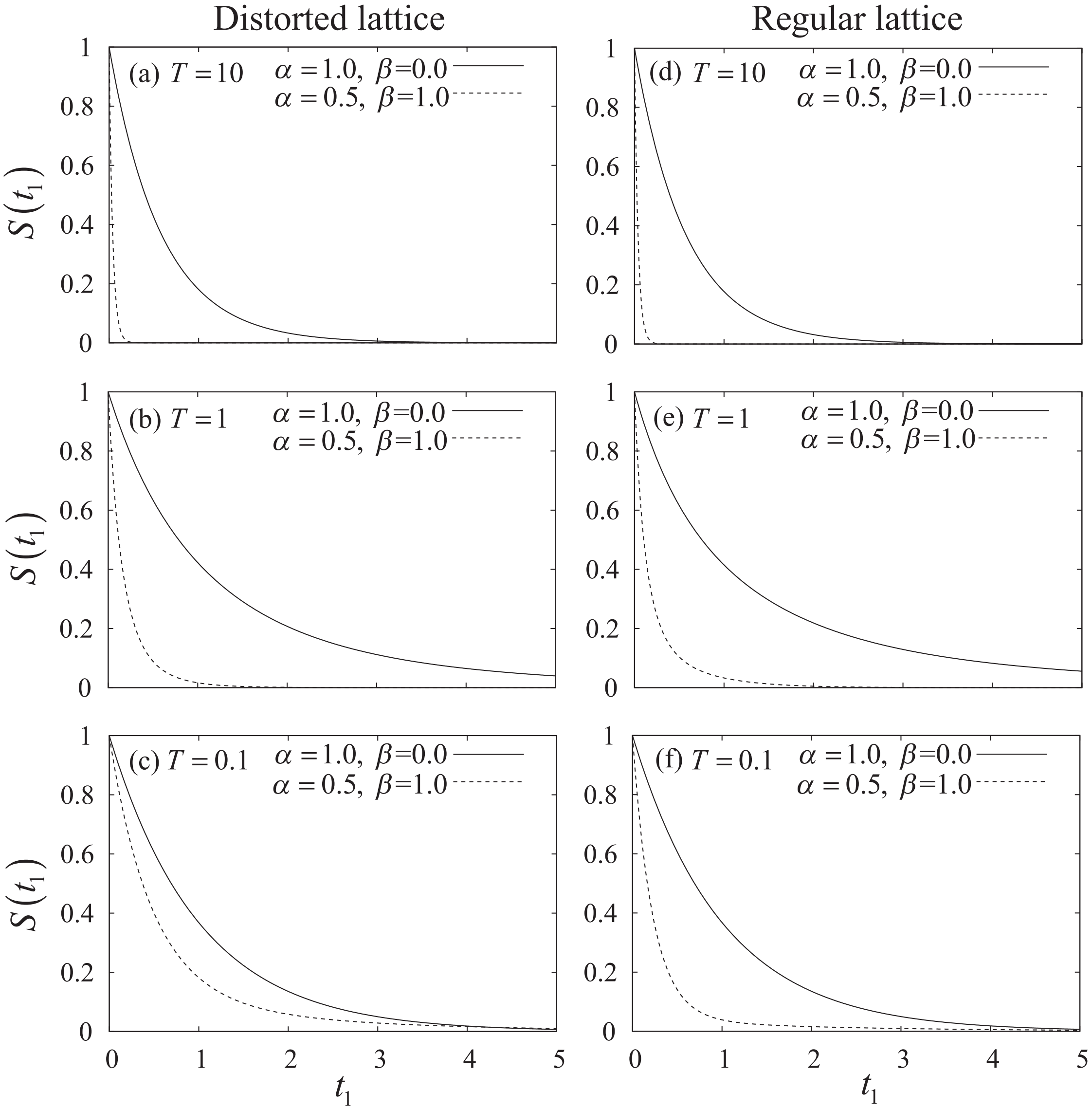

Figure 4.4: The linear absorption (1D) signals $S(t_1)$ for (i) single flip case, $\alpha=1$ and $\beta=0$ (solid line), and (ii) single-double mixed flips case, $\alpha=0.5$ and $\beta=1$ (dashed line), are plotted for the same sets of parameters $\langle \delta\mathbf{a}_j^2 \rangle$ and T used in Fig. 4.2. The intensities of the signals are normalized by their initial values.

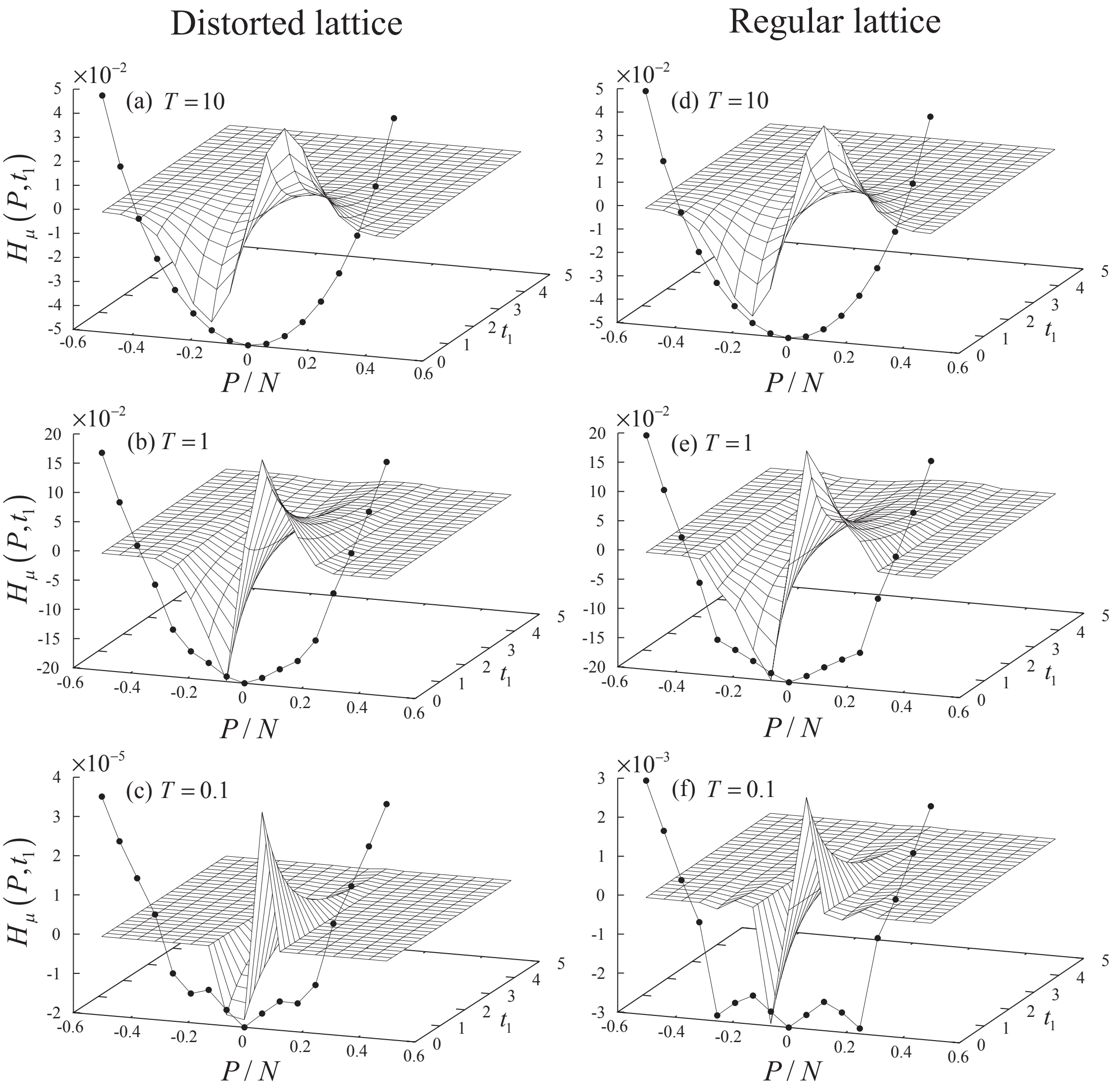

Figure 4.5: The time evolution of $H_{\mathbf{\mu}}(P,t_1)$ for the single-flip dynamics for the distorted cases (a)-(c), and the regular cases (d)-(f), at different temperatures in the same order of Fig. 4.2. The line above the P axis shows the corresponding FEL.

B. Two-Dimensional Signals

While we couldn't observe any features specific to the FELs from 1D measurements, we have investigated their third order response function $S\left(t_3,0,t_1\right)$. We plot contour maps of 2D signals defined by $S\left(t_3,0,t_1\right)$ for the distorted and regular lattice cases at different temperatures in the same order as in Fig. 4.2. Figure 4.6 is for single-flip ($\alpha=1,\beta=0$), while Fig. 4.7 is for single-double mixed flips ($\alpha=0.5,\beta=1.0$) dynamics. Compared with the 1D case, 2D spectroscopy is much more sensitive to the difference of temperatures, configurations of dipoles, and dynamics. As can be seen in Figs. 4.2(a) and 4.2(d), the FELs at the high temperature are similar due to the entropic contributions. The corresponding 2D signals in Figs. 4.6 (a) and 4.6(d) or Figs. 4.7(a) and 4.7(d) show a similar 2D profile, if we normalize the time scales by the relaxation times estimated from Fig. 4.4. First we should notice that if the dipole element of the laser interaction is a linear function of the system polarization *P*, the 2D signals will be vanished for a harmonic potential due to the destructive interference of the multiple laser excitations.[86] Although there is always a quartic anharmonicity in the FELs as illustrated in Eq. (4.4.6), its contribution is too small to have the signals comparable to the calculated results. In the present case, it is the nonlinearity that causes 2D signals for the high temperature parabolic potential. Based upon the profile analysis between the initial equilibrium distribution and the laser excited distribution depicted in Fig. 4.5, we have found the effective dipole element in the laser interactions is not linear but linear with the cubic function expressed as $P-\varepsilon P^3$, where ε is the constant in the order of 10^{-2}. The nonlinear contribution arises because we have constructed the dipole operator non-kinetic way by expanding the Liouville operator with the external interaction defined with the Boltzmann factors.

Regardless of the form of the laser interaction, the decays of signal profiles reflect the system dynamics, since the time-evolutions of the system between the excitations are governed by the system Liouvillian only. Thus, the 2D profiles in the high temperature case decay monotonically as the function of t_1 and t_2. For the intermediate and lower temperature cases as shown in Figs. 4.2(b), 4.2(c), 4.2(e) and 4.2(f), the anharmonicity of potential is strong and the primary cause of the signals is the anharmonicity of the FELs rather than the nonlinearly of dipole. While the signals for the distorted and regular cases exhibit similar profiles at high temperature as shown in Figs. 4.6(a) and (d) and in Figs. 4.7(a) and (d), they show clear differences at low temperature as illustrated in Figs. 4.6(c) and (f) and in Fig. 4.7(c) and (f). These signals seem to reflect the differences of the FEL profiles presented in Fig. 4.2, indicating a possibility to detect a profile of FEL. The sensitivity of 2D spectroscopy also suggests a possibility to detect the difference of dynamics on the same FELs, since the profiles depicted in Figs. 4.6 and 4.7 are different if the dynamics is different even it is governed by the same FELs.

To see underlying dynamics on 2D signals, we plot the distribution given in Eq. (4.3.11). Figures 4.8(a)-(f) illustrate $H_{\mu\mu\mu}\left(P, t_3, 0, t_1\right)$ with $t_1 = 0$ in the same order as Figs. 4.2(a)-(f) for the single flip dynamics. Although $H_{\mu\mu\mu}\left(P, t_3, 0, t_1\right)$ is not an observable, it is as sensitive as 2D signals for the difference of dynamics. Thus, $H_{\mu\mu\mu}\left(P, t_3, 0, t_1\right)$ for the single-double flips case exhibits some differences from the single flip case presented in Fig. 4.8 unlike the case of 1D spectroscopy. Since a role of FEL can be sufficiently explained from the single flip case, here we display the single flip case only.

For the high temperature cases shown in Figs. 4.8(a) and (d), the distribution profiles decay monotonically reflecting the monotonic decays of signals observed in Figs. 4.6(a) and (d). Similar behaviors are observed in Figs. 4.7(a) and (d). The differences between Figs. 4.6(a) and (d) and 4.7(a) and (d) are their time scales which can be adjusted by the relaxation time estimated from Fig. 4.4(a) and (d). While the FELs of distorted and regular cases appear similar at high-temperature due to the entropic contribution, they become different at low temperature, which reflects the differences in the system energetics. These differences in FELs seem to be detected by 2D spectroscopy as illustrated in Figs. 4.6(b) and (e) as well as 4.7(b) and (e). The relaxations of distributions presented in Figs. 4.8(b) and 4.8(e) are no longer monotonic, because the multiple excitations involved in 2D spectroscopies excite various modes with different relaxation constants. Since the role of relaxation depends on the time sequence t_1 and t_3, the 2D spectroscopy can provide more information than 1D spectroscopy.

When the temperature becomes very low, a remarkable difference appears between the distorted and regular cases. This difference can be easily explained by comparing the time-evolution of $H_{\mu\mu\mu}\left(P, t_3, 0, t_1\right)$ as shown in Figs. 4.8(c) and (f). The elongation of the peak in the t_3 directed in Fig. 4.6 (f) can be attributed to the trapping of the distribution in the local minima around $P/N = \pm 0.25$ as illustrated in Fig. 4.8(f). We also have observed the trapping of $H_{\mu\mu\mu}\left(P, t_3, 0, t_1\right)$ in the single-double mixed flips case (not shown), but the trapped distribution decays more quickly than the single flip case and the elongated contribution in Fig. 4.7(f) is much smaller than that in Fig. 4.6(f). Since other 2D signals do not show the elongation, this implies the local minimum of the FEL may be detected as the elongated peak in the t_3 direction in the 2D IR spectroscopy.

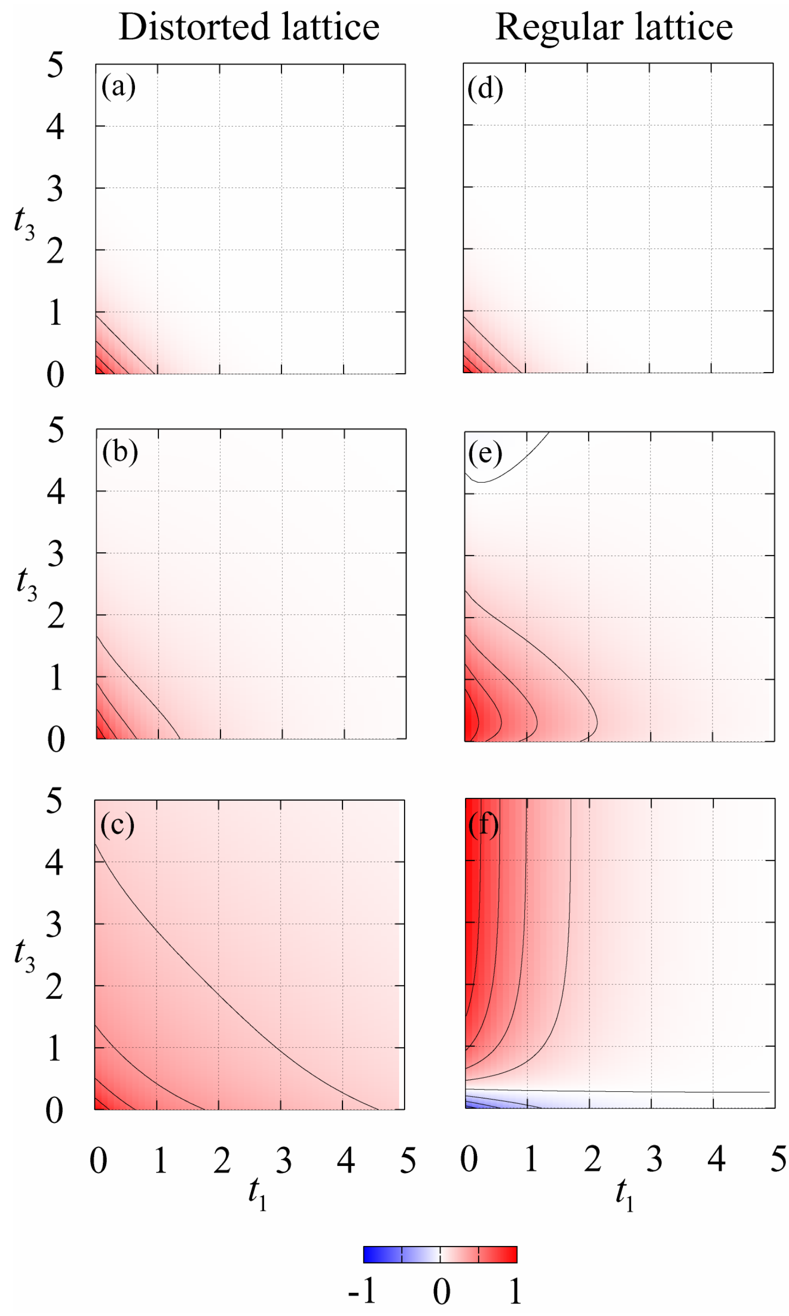

Figure 4.6: The contour maps of the 2D signals for the single-flip dynamics. The intensity of each plot is normalized by its maximum or minimum value.

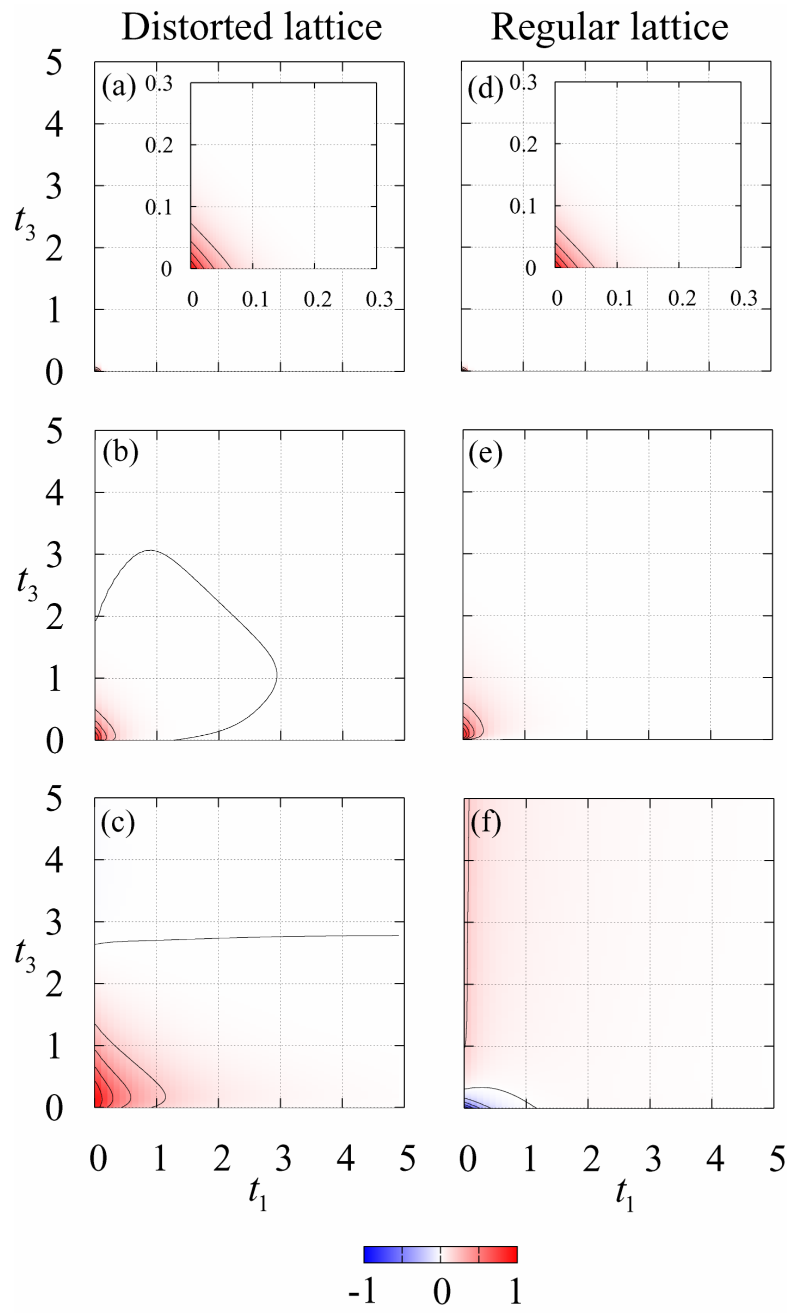

Figure 4.7: The contour maps of the 2D signals for the single-double mixed flips dynamics $(\alpha = 0.5, \beta = 1)$. The intensity of each plot is normalized by its maximum or minimum value. The insets of Figs. 4.7(a) and (d) show $S(t_3, 0, t_1)$ by using the magnified scale.

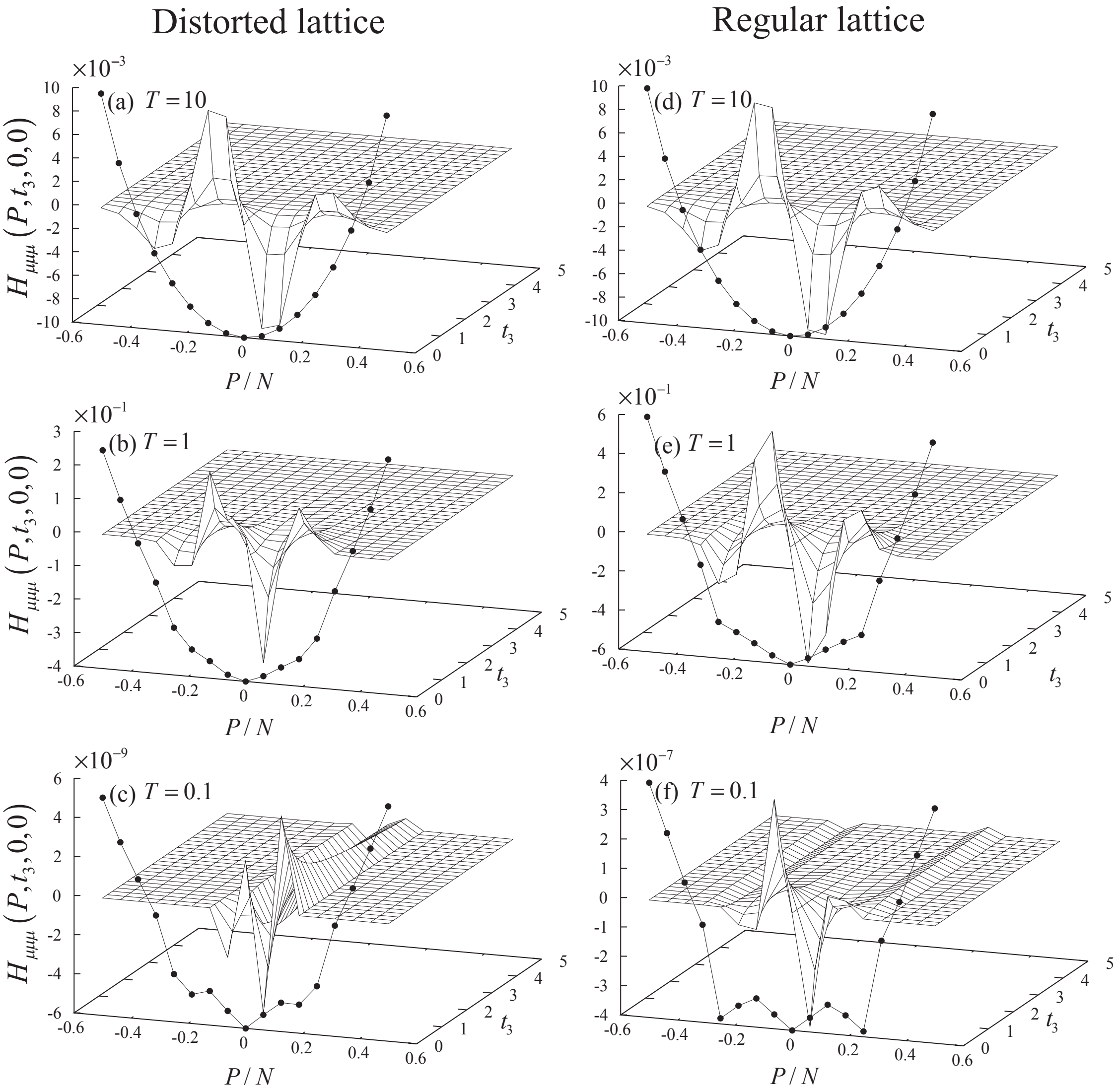

Figure 4.8: The time evolution of $H_{\mu\mu\mu}(P,t_3,0,t_1)$ for the single-flip dynamics with $t_1=0$ for the distorted cases (a)-(c), and the regular cases (d)-(f), at different temperatures in the same order of Figs. 4.2(a)-(f). The line above the P axis shows the corresponding FEL.

4.6 Smoluchowski Equation Approach

To discuss dynamical behaviors of FELs, a time-dependent Ginzburg-Landau (TDGL) equation approach [11][12][13] and Smoluchowski equation approach [125][126] are often used by assuming a driving force of macroscopic coordinate X which is proportional to the gradient of the free energy $dF(X)/dX$. For a simple model of electron transfer (ET) problem, a relationship between the master equation and the Smoluchowski equation approaches has been clarified for the high temperature case [61], but the validity of such equation of motion approaches for the low temperature case has not been examined. Here, we examined the applicability of the Smoluchowski equation approach by calculating 1D and 2D signals for the FELs given in Figs. 4.2(a)-(f) and compared with the microscopically calculated 1D and 2D signals presented in Sec. 4.5.

For the distribution $H\left(P,t\right)$, the Smoluchowski equation is expressed as

$$\frac{\partial}{\partial t}H\left(P,t\right)=-\mathbf{L}_S H\left(P,t\right). \tag{4.6.1}$$

The Liouville operator is given by

$$-\mathbf{L}_S = D\left[\frac{1}{k_B T}\frac{\partial}{\partial P}\left(\frac{\partial F\left(P\right)}{\partial P}\right)+\frac{\partial^2}{\partial P^2}\right], \tag{4.6.2}$$

where D is the diffusion constant. The Smoluchowski equation describes the same dynamics as the overdamped limit of the Langevin dynamics with the white noise fluctuations. In the Smoluchowski case, the dynamics is described as the probability diffusion on the potential $F\left(P\right)$. As in the case of ET problem, one can relate to the microscopic master equation approach and phenomenological Smoluchowski equation approach if the system is in the high temperature case. In Appendix B, we deduce the Smoluchowski equation for the single flip and the single-double flips master equations at the high temperature. Thus, in the high temperature case, we can estimate the coefficients in Eq.(4.6.2) directly from the master equation. Note that, as shown in Appendix B, the single flip and single-double flips dynamics of the master equation approach can be treated uniformly in the Smoluchowski equation approach as the choice of diffusion parameters. Since the phenomenological features do not depend on the diffusion parameters, here discuss the single flip case only to examine the validity of Smoluchowski equation.

To calculate 1D and 2D signals, we need to define the dipole operator. As mentioned in Sec. 4.5, the dipole element introduced in the master equation approach contains the cubic polarization term. We consider the free energy with the electric perturbation expressed as $F(P)-B\left(P+\varepsilon P^3\right)$, where B is a weak electric field and a small constant. When we expand the free energy up to the first order by the perturbation, we have the dipole operator in the form

$$\boldsymbol{\mu}_s=-\frac{D}{k_B T}\left[\frac{\partial}{\partial P}+\varepsilon\left(6P+3P^2\frac{\partial}{\partial P}\right)\right], \tag{4.6.3}$$

where we evaluate $\varepsilon=-0.03$ from the master equation approach. Replacing the Liouvillian and dipole operator in Eqs.(4.3.10) and (4.3.11) by those in Eqs.(4.6.2) and (4.6.3), we can calculate the 1D and 2D signals from the Smoluchowski approach. Note that the equilibrium state in the Smoluchowski approach is given by $\rho_{eq}\propto\exp\left(-F(P)/k_B T\right)$. In Figs. 4.9(a)-(c), we plot the 1D signals calculated from the Smoluchowski approach for the FELs given in Figs. 4.2(a)-(f). In each figure, the solid and dashed lines represent the distorted and regular lattice cases, respectively. The nonlinearlity of the dipole element does not play a major role in the 1D case, since it gives rise to a minor collection of the signals. We adjust the diffusion constants to fit the results from the single flip master equation dynamics. For the high temperature case, we use $D=7.14$ for the distorted and regular lattices which roughly agrees with the value reduced from the master equation. In the high temperature case in Fig.4.9(a) where the FEL profile becomes parabolic, we can analytically evaluate the 1D signals from Smoluchowski approach as described in Appendix C and the single exponential decay of the signals, which was also observed in the master equation approach, is explained as the relaxation of the harmonic mode. For the intermediate and low temperature cases shown in Figs. 4.9(b) $T=1$ and 4.9(c) $T=0.1$, respectively, the relaxation constants for the distorted and regular lattices are evaluated as (b) $D = 1.67$ (solid line) and $D = 2.50$ (dashed line) and (c) $D = 0.010$ (solid line) and $D = 0.028$ (dashed line). While all curves in Fig. 4.9(b) can be fitted by a simple exponential function, the curves in Fig. 4.9(c) are expressed by the sum of exponential functions, which are different from the microscopic results given in Figs. 4.4(b), (c), (e) and (f).

The 2D signals calculated from the Smoluchowski equation at different temperatures are presented in Figs. 4.10(a)-(f). As mentioned in Sec. 4.5, the 2D signals in the high temperature case arise from the nonlinearity of the dipole elements. If we calculate the 2D signals with setting $\varepsilon = 0$ for a harmonic potential with quartic anharmonicity using the Smoluchowski equation, the signals become negative and give a different 2D profile as shown in Fig. 4.11. This fact supports the form of dipole given in Eq.(4.6.3). While the Smoluchowski equation well reproduces the 1D signals at all temperatures and the 2D signals at high temperature calculated from the master equation, it cannot simulate the 2D signals in the low temperature cases as shown in Figs. 4.10 (b), (c), (e) and 4.10(f). For these figures, we have used the same relaxation constant D as used for the dashed and solid lines of Figs. 4.9(a)-(c). Although we have changed D as well as the nonlinearlity of dipole ε, we could not reproduce profiles similar to those found in Figs. 4.6. This result indicates that the applicability of the Smoluchowski equation is limited to the high temperature case, where the FEL profile is parabolic. We should address that this limitation becomes prominent due to the sensitivity of 2D spectroscopy.

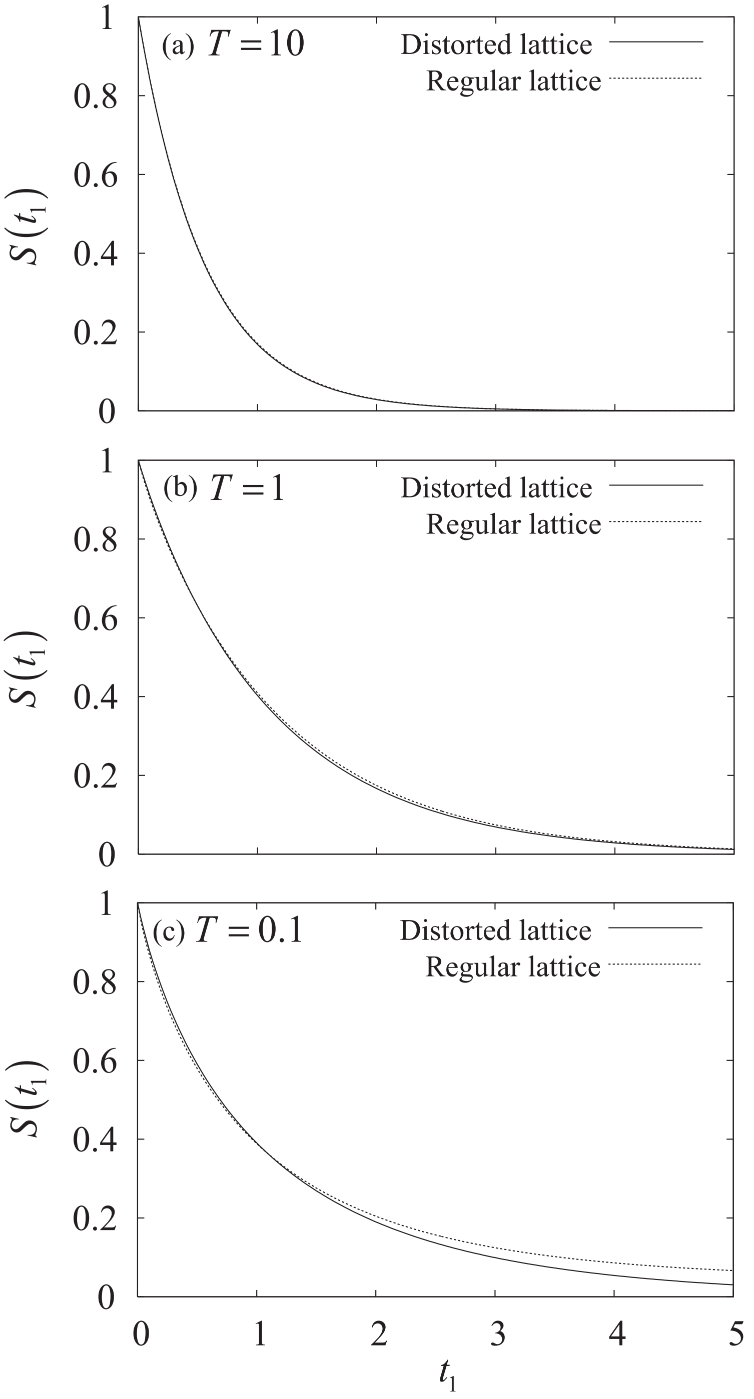

Figure 4.9: The 1D signals calculated from the Smoluchowski approach for the FELs given in Fig. 4.2(a)-(f): (a) $T = 10$ for the high temperature case, (b) $T = 1$, for the middle temperature case and $T = 0.1$ for the low temperature case. In each figure, the solid and dotted lines represent the distorted and regular lattice cases, respectively.

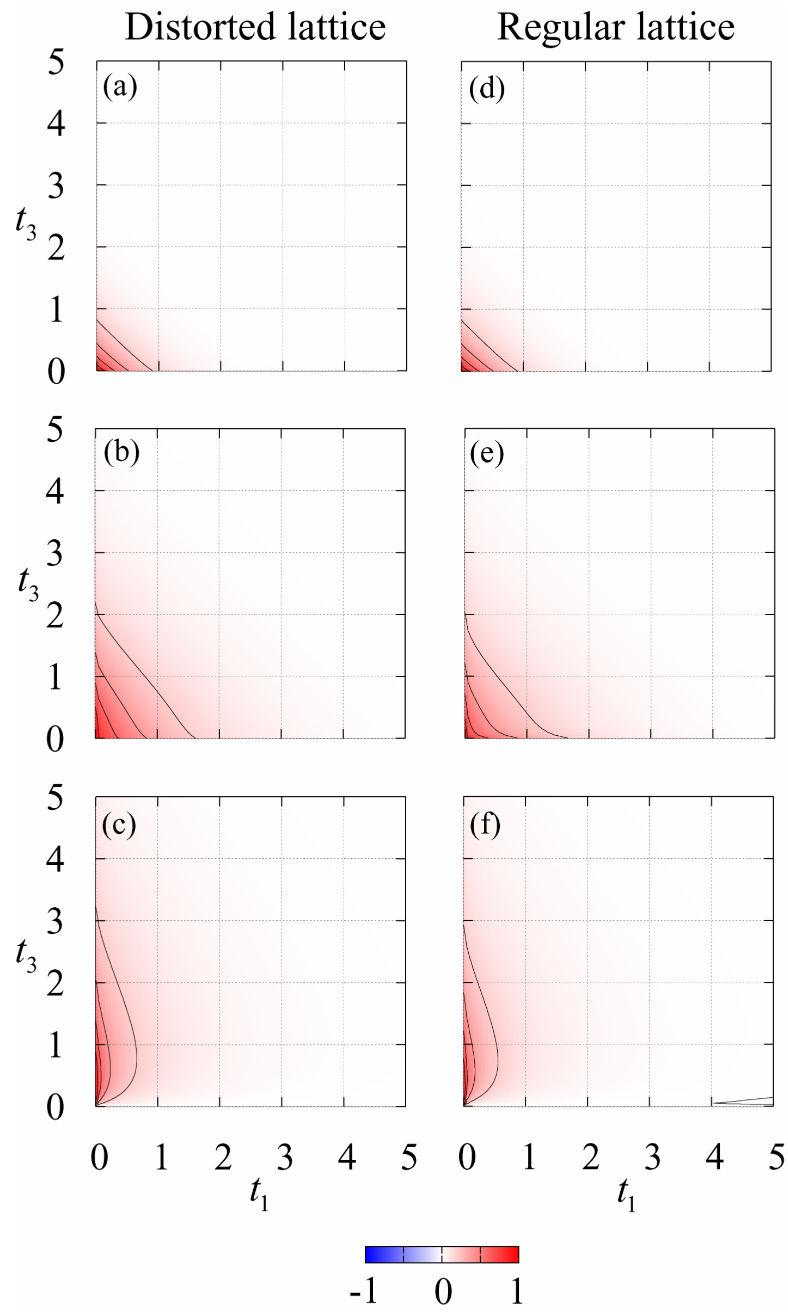

Figure 4.10: The contour maps of the 2D signals calculated from the Smoluchowski equation with the nonlinear excitation for the distorted cases (a)-(c), and the regular lattice cases (d)-(f), at different temperatures in the same order of Figs 4.2(a)-(f). The intensity of each plot is normalized by its maximum.

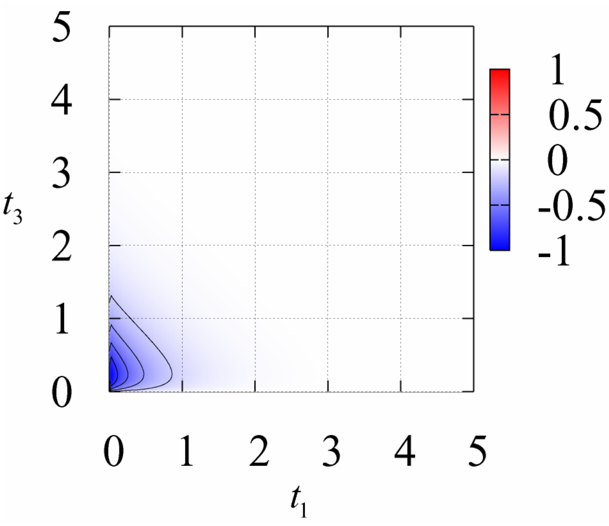

Figure 4.11: The contour map of the 2D signal calculated from the Smoluchowski equation without the nonlinear excitation ($\varepsilon = 0$) for the high temperature case. The intensity of the plot is normalized by its minimum.

4.7 Conclusion

Having employed a simple model for the regular and the distorted dipolar systems, we are able to have the exact FEL and collective dynamics of the system at any temperatures, which allows us to explore a possibility to obtain information on the FEL by spectroscopic means. The evaluated FEL exhibits the parabolic shape at high temperature whereas it shows a bumpy profile with some minima at low temperature, where the motion of dipoles is frozen. From the master equation approach, we calculated the 1D and 2D singles for single flip and single-double flips dynamics. While the 1D signals were characterized by the featureless exponential or sum of exponential relaxation signals regardless of the FEL profiles, 2D spectra showed distinct differences for different FEL profiles. The local minima of the FEL were detected as the elongation of 2D signals in the t_3 direction. This indicates that 2D spectroscopy may be a useful tool to analyze FEL profile expressed as the function of system polarization.

To examine the validity of Smoluchowski equation, we also have calculated the 1D and 2D spectra using the microscopically calculated FELs. For the high temperature case, the dynamics described by the master equation and Smoluchowski equation was essentially the same for the large system size thus their calculated 1D and 2D signals were the same. However, in the middle and low temperature cases, these signals were different, which indicates that Smoluchowski equation might not be accurate to describe the dynamics for the system with nonparabolic FELs.

Finally, we should address the limitation of the present analysis. To have the accurate FEL with the decreasing the degrees of freedom, we had to discretize the configuration of dipoles, which made the employment of kinetic dynamics impossible. We thus employ the stochastic dynamics using the master equation. To make our statement more concrete, we have to compare the present results with the kinetic ones. For instance, although the Smoluchowski equation reproduces the stochastic results only in the high temperature case, our statement for dynamics on the FEL may change if we consider the kinetic system. The model dependence as well as the size dependence of the present results has not been explored, which is essential to discuss a real system.

Chapter 5
Conclusion

We have analyzed the free energy landscapes (FELs) for three types of models representing ionic solvation, electron transfer (ET) and dipolar crystal systems in terms of statistical and dynamical aspects. In general, the FEL is a useful concept for explaining the static and dynamic behaviors of systems since it corresponds to the probability of achieving a given state, and is well characterized by a simple functional form even with complex interactions among atoms and molecules at high temperature. One of our research interests is the structural change of the FEL depending on the physical conditions such as temperature. For obtaining reasonable FELs, we introduced models to decrease the degree of freedom and employed suitable calculation method, Wang-Landau method.

The Chapter 2, a simulation model for ionic solvation in a polar solvent is prepared, in which a central charge is surrounded by dipolar molecules posted on the distorted lattice sites with simple rotational dynamics. The density of states is calculated by applying the Wang-Landau algorithm to both the energy and polarization states. The FELs of solvent molecules as the function of polarization are depicted to explore the competition between the thermal fluctuation and solvation energy. Without the central charge, for temperatures higher than the energy scale of the dipole-dipole interactions, the energy landscape for the small polarization region exhibits a parabolic shape as predicted by Marcus for ET reaction, while there is an additional quartic contribution to the landscape for the large polarization region. When the temperature drops, the simulated FELs are no longer smooth due to the presence of multiple local minima arising from the frustrated interactions among the dipoles. The parabolic contribution becomes negligible and the energy landscape becomes quartic in shape. If the central charge is strong, the energy landscape exhibits an asymmetric profile due to the contributions of linear and cubic terms that arise from the charge-dipole interactions.

In Chapter 3, a model to simulate electron transfer (ET) reaction is prepared with a solute dipole surrounded by dipolar molecules with simple rotational dynamics posted on the three-dimensional distorted lattice sites. The interaction energy between the solute and solvent dipoles as a reaction coordinate is adopted and FELs are calculated by generating all possible states for a 26-dipolar-system and by employing Wang-Landau sampling algorithm for a 92-dipolar-system. For temperatures higher than the energy scale of dipole-dipole interactions, the FELs for the small reaction coordinate region have the quadratic shape as predicted by Marcus, whereas for the large reaction coordinate region, the shape of the landscapes is non-quadratic. When the temperature drops, small notched structures appear on the free energy profiles because of the frustrated interactions among the dipoles. The formation of notched structure is analyzed with statistical approach and it is shown that the amplitude of notched structure depend upon the segment size of the reaction coordinate and is characterized by the interaction energy among the dipoles. Using simulated FELs, we calculate the reaction rates as a function of the energy gap for various temperatures. At high temperatures, the reactions rates follow a bell shaped (inverted parabolic) energy gap law in the small energy gap regions, while the bell shape becomes steeper than the parabolic shape in a large energy gap regions due to the FEL’s non-quadratic shape. The peak position of the parabola also changes as the function of temperature. At low temperatures, the profile of the reaction rates is no longer smooth because of the many local minima of the FELs.

The other interest of our research is to explore the relationship between FEL and system dynamics. The FEL corresponds to the thermal fluctuation of the system, however the FEL does not perfectly govern the system dynamics. This is because the FEL is defined by the thermal equilibrium state where the dynamical behaviors become invisible. In addition, the FEL is a highly conceptual quantity because it is not directly observable. Thus we introduced a model which enables us to calculate both static and dynamic quantities and to attempt to explain the system dynamics on the FEL by means of linear and nonlinear IR spectroscopies.

In Chapter 4, a model for the dipolar crystal system is employed to explore a role of FEL, in which dipolar molecules are posted on two-dimensional lattice sites with two-state librational dynamics. All dipole-dipole interactions are included to have frustrated interactions among the dipoles. For the regular and distorted lattice cases, the FEL is calculated from the interaction energies and the total polarizations for all possible dipolar states at various temperatures. At high temperature, the shape of the calculated FEL is smooth and parabolic, while it becomes bumpy at low temperature exhibiting multiple local minima. To study dynamical aspects of the system, the single flip dynamics and the single-double mixed flips dynamics of dipoles are examined from a master equation approach. As the observables of linear absorption and two-dimensional (2D) infrared and far infrared spectroscopies, the first- and third-order response functions of polarization are calculated for different physical conditions characterized by the FEL. While the linear absorption signals decay in time in a similar manner regardless of the FEL profiles, the 2D signals exhibit prominent differences for those profiles. This indicates that, we may differentiate the FEL profiles by changing two-time valuables in 2D spectroscopy. As illustrated in the single-double flips case, the FEL study by means of 2D spectroscopy, however, depends on the dynamics which is set independently from the FEL. The Smoluchowski equation is applied to examine the description of the collective dynamics on the microscopically calculated FEL. We found that the 1D and 2D signals calculated from the Smoluchowski equation agree with those from master equation only at the temperatures where the FELs become parabolic shape.

Appendix A
Brief Summary of Random Energy Model (REM)

In a framework of the random energy model (REM)[58][59], all dipole-dipole and charge-dipole interactions are assumed to have a random Gaussian distribution function characterized by the averaged charge-dipole and dipole-dipole interactions $\bar{\xi}(q)$ and $\bar{J}$, and their standard deviations $\Delta\xi$ and ΔJ. The average solvation energy is then given by,

$$\bar{E}(x) = N\left[x\bar{\xi}(q) + z\bar{J}x^2\right], \tag{A.1}$$

where z is the average number of dipoles interacting with each single dipoles. The standard deviation of the solvation energy is assumed to be independent of x and given by

$$\Delta E^2 = N\left[\Delta\xi^2 + z\Delta J^2\right]. \tag{A.2}$$

Introducing the probability distribution $g(x,E)$ at polarization x as

$$g(x,E) = \frac{1}{\sqrt{2\pi}\Delta E}\exp\left[-\frac{\left(E-\bar{E}(x)\right)^2}{2\Delta E^2}\right] \tag{A.3}$$

yields an average density of states with polarization x and energy between E and $E+dE$

$$\left\langle n(x,E)\right\rangle = \Omega(Nx)\,g(x,E), \tag{A.4}$$

where

$$\Omega(Nx) = \frac{N!}{n_+!n_-!} = \frac{N!}{\left[N(1-x)/2\right]!\left[N(1+x)/2\right]!} \tag{A.5}$$

is the total number of states with polarization x. For $\langle n(x,E)\rangle >> 1$, one can approximate $\langle \ln n(x,E)\rangle$ by $\ln\langle n(x,E)\rangle$, and the entropy can be written by

$$S(x,E) \approx \ln\left\langle n(x,E)\right\rangle = \ln\Omega(Nx) - \frac{\left(E-\bar{E}(x)\right)^2}{2\Delta E^2} - \ln\left(\sqrt{2\pi}\Delta E\right). \tag{A.6}$$

The above approximation is not valid below the critical energy,

$$E_c \approx \bar{E}(x) - \Delta E\left(2\ln(Nx)\right)^{1/2} \tag{A.7}$$

since the entropy becomes negative. Therefore we set $S(x,E)=0$ for $E<E_c(x)$. This result indicates a polarization-dependent phase transition at the temperature

$$T_c(x) = \frac{\Delta E}{S^*(Nx)}, \tag{A.8}$$

where the configuration entropy $S^*(Nx)$ is given by $S^*(Nx)=\log(\Omega(Nx))$. In the large N limit, the configuration entropy becomes

$$S^*(Nx) = N\left[-\left(\frac{1+x}{2}\right)\ln\left(\frac{1+x}{2}\right)-\left(\frac{1-x}{2}\right)\ln\left(\frac{1-x}{2}\right)\right] \tag{A.9}$$

with the aid of the Stirling's formula. Then the free energy landscape for REM approximation is expressed as

$$F_{\mathrm{REM}}(x,T) = \begin{cases} \dfrac{1}{N}\left(\bar{E}(x) - \dfrac{\Delta E^2}{2T} - TS^*(Nx)\right) & T > T_c(x) \qquad \text{(A.10)} \\ \dfrac{1}{N}\left(\bar{E}(x) - \Delta E\left(2S^*(Nx)\right)^{1/2}\right) & T \le T_c(x) \qquad \text{(A.11)} \end{cases}$$

To determine the average number of interacting dipoles z for dipole-dipole interactions, which affects long range, we use the following condition:

$$F(1,T)/N = F_{\mathrm{REM}}(1,T)/N = \bar{E}(1)/N \tag{A.12}$$

Note that, in Eq. (A.12), we always use the free energy for $T \le T_c(x)$ because $T_c(x)$ becomes infinite when $x \to 1$.

Appendix B
Derivation of the Smoluchowski Equation

In this Appendix, we discuss the relation between the master equation and the Smoluchowski equation. The time evolution of our system is given by the master equation Eq. (4.3.1) and the probability distribution vector $\vec{\rho}(t)$ has 2^N states. Here we rewrite the Eq. (4.3.1) as the following form

$$\frac{\partial}{\partial t}\rho_i(t)=\sum_j\left[(-\mathbf{L})_{i,j}\,\rho_j(t)-(-\mathbf{L})_{j,i}\,\rho_i(t)\right]. \tag{B.1}$$

For the high temperature case, the transition occurs absolutely if two states are connected with given dynamics, thus the transition matrix, $-\mathbf{L}=-\alpha\mathbf{L}^{(1)}-\beta\mathbf{L}^{(2)}$, can be written as

$$(-\mathbf{L})_{i,j}=\alpha C_{i,j}^{(1)}+\beta C_{i,j}^{(2)}, \tag{B.2}$$

where $C_{i,j}^{(n)}$ is the connectivity coefficient introduced in the section 4.3. Assuming a single flip and double flips of dipole in the system whose polarization is P_j, we can construct the rate equation expressed as

$$\begin{aligned}\frac{\partial}{\partial t}\rho_{i,P_i}(t)=&-\alpha N\rho_{i,P_i}(t)+\alpha\sum_j\rho_{j,P_j}(t)C_{i,j}^{(1)}\delta\left(P_i-\{P_j-\Delta P\}\right)\\&+\alpha\sum_j\rho_{j,P_j}(t)C_{i,j}^{(1)}\delta\left(P_i-\{P_j+\Delta P\}\right)\\&-\beta\frac{N(N-1)}{2}\rho_{i,P_i}(t)+\beta\sum_j\rho_{j,P_j}(t)C_{i,j}^{(2)}\delta\left(P_i-\{P_j-2\Delta P\}\right)\\&+\beta\sum_j\rho_{j,P_j}(t)C_{i,j}^{(2)}\delta\left(P_i-P_j\right)+\beta\sum_j\rho_{j,P_j}(t)C_{i,j}^{(2)}\delta\left(P_i-\{P_j+2\Delta P\}\right)\end{aligned}, \tag{B.3}$$

where $\rho_{i,P_i}(t)$ is the *i*th component of the probability distribution vector $\vec{\rho}(t)$ and the subscript P_i is introduced for representing the polarization of the *i*th state. Here we calculate the polarization and time probability distribution function $H(P(k),t)$ by summing Eq.(B.3) over all states with the same polarization $P(k)$. Operating $\sum_i\delta_{P(k),P_i}$ to both sides of Eq.(B.3), we obtain

$$\begin{aligned}\frac{\partial}{\partial t}H\left(P(k),t\right)=&-\left[\alpha N+\beta\left(\frac{N^2}{4}-\frac{N}{2}+k^2\right)\right]H\left(P(k),t\right)\\&+\alpha\left(\frac{N}{2}+1-k\right)H\left(P(k)-\Delta P,t\right)\\&+\alpha\left(\frac{N}{2}+1+k\right)H\left(P(k)+\Delta P,t\right)\\&+\beta\left\{\frac{N^2}{8}+\frac{3N}{4}+1+\frac{1}{2}\left[k^2-k(N+3)\right]\right\}H\left(P(k)-2\Delta P,t\right)\\&+\beta\left\{\frac{N^2}{8}+\frac{3N}{4}+1+\frac{1}{2}\left[k^2+k(N+3)\right]\right\}H\left(P(k)+2\Delta P,t\right)\end{aligned}\quad. \tag{B.4}$$

Here assuming $P(k)$ be continuous variable and taking large N limit, we get

$$\frac{\partial}{\partial t}H(P,t)=\left(\gamma\frac{\partial}{\partial P}P+D\frac{\partial^2}{\partial P^2}\right)H(P,t), \tag{B.5}$$

where we set $\gamma=2(\alpha+N\beta)$ and $D=N\Delta P^2(\alpha+N\beta)/2$. The first and second terms correspond to the drift term and diffusion terms, respectively.

Appendix C

Linear Absorption Signal from Smoluchowski Equation Approach

If the potential is harmonic, the Smoluchowski equation for a given arbitrary initial condition can be easily solved as

$$H\left(P,t\right)=\sum_{n=0}a_n\exp\left(-n\gamma t\right)\exp\left(-\frac{\gamma}{2D}P^2\right)H_n\left(\sqrt{\frac{\gamma}{2D}}P\right),\tag{C.1}$$

where $H_n\left(\xi\right)$ are the Hermite polynomials and a_n are the initial values for nth eigenfunctions. For 1D spectroscopy, the nonlinearity of dipole plays a minor role, so we can set $\varepsilon=0$ in Eq.(4.6.3). At high temperature, the FEL is approximated by parabolic function, so that the initial condition of the Smoluchowski immediately after excitation is expressed by the first Hermite polynomial, i.e. $H\left(P,0\right)\sim\exp\left(-\xi^2\right)H_1\left(\xi\right)$, where $\xi=\sqrt{\gamma/2D}P$. Thus, the 1D signal for high temperature is analytically evaluated as

$$S\left(t_1\right)\sim\exp\left(-\gamma t\right)\int dP\exp\left(-\frac{\gamma}{2D}P^2\right)H_1\left(\sqrt{\frac{\gamma}{2D}}P\right).\tag{C.2}$$

This equation indicates the signal decays exponentially as the relaxation of collective mode with the relaxation rate γ.

References

1 C. A. Angell, K. L. Ngai, G. B. McKenna, P. F. McMillan, S. W. Martin, J. Appl. Phys. **88**, 3113 (2000).

2 P. Welch and M. Muthukumar, .Phys. Rev. Lett. **87**, 218302 (2001).

3 R. A. Marcus, Rev. Mod. Phys. **65**, 599 (1993).

4 R. A. Marcus, J. Chem. Phys. **24**, 966 (1956); 979 (1956).

5 C. L. Brooks III, M. Gruebele, J. N. Onuchic, and P. G. Wolynes , Proc. Natl. Acad. Sci. USA, **95**, 11037 (1998).

6 D. J. Wales, *Energy Landscapes*, (Cambridge University Press, 2004).

7 D. J. Wales and T. V. Bogdan, J. Phys. Chem. B, **110**, 20765 (2006).

8 C. Chipot and A. Pohorille, Free Energy Calculations, (Springer-Verlag Berlin Heisenberg, 2007).

9 L. D. Landau, Phys. Z. Sowjet., **11**, 26 (1937); **11**, 545 (1937).

10 M. Mézard, G. Parisi, and M. A. Virasoro, *Spin Glass Theory and Beyond* (World Scientific, Singapore, 1987).

11 M. Cyrot, Reports on Progr. Phys. **36**, 103 (1973).

12 K. Kawasaki, M. C. Yalabik, and J. D. Gunton, Phys. Rev. A, **17**, 455 (1978).

13 S. Noguchi and T. Ohta, J. Phys. Soc. Jpn. **72**, 1315 (2003).

14 J. R. Miller, L. T. Calcaterra, and G. L. Closs, J. Am. Chem. Soc. **106**, 3047 (1984).

15 M. R. Wasielewski, M. P. Niemczyk, W. A. Svec and E. B. Pewitt, J. Am. Chem. Soc. **107**, 1080 (1985).

16 N. Mataga, T. Asahi, Y. Kanda, T. Okada and T. Kakitani, Chem. Phys. **127**, 249 (1988).

17 D. F. Calef and P. G. Wolynes, J. Phys. Chem. **87**, 3387 (1983).

18 D. F. Calef and P. G. Wolynes, J. Chem. Phys. **78**, 470 (1983).

19 M. Tachiya, J. Phys. Chem. **93**, 7050 (1989).

20 A. Yoshimori, T. Kakitani, Y. Enomoto, and N. Mataga, J. Phys. Chem. **93**, 8316 (1989).

21 J. K. Hwang and A. Warshel, J. Am. Chem. Soc. **109**, 715 (1987).

22 R. A. Kuharski, J. S. Bader, D. Chandler, M. Sprik, M. L. Klein, and R. W. Impey, J. Chem. Phys. **89**, 3248 (1988).

23 E. A. Carter and J. T. Hynes, J. Phys. Chem. **93**, 2184 (1989).

24 K. Ando and S. Kato, J. Chem. Phys. **95**, 5966 (1991).

25 Y. Suzuki and Y. Tanimura, J. Chem. Phys. **124**, 124508 (2006).

26 Y. Suzuki and Y. Tanimura, J. Chem. Phys. **126**, 054504 (2007).

27 G. Diezemann, U. Mohanty, and I. Oppenheim, Phys. Rev. E, **59**, 2067 (1999).

28 T. Odagaki, T. Yoshidome, A. Koyama, and A. Yoshimori, J. Non-Cryst. Solids **352**, 4843 (2006).

29 G. Adjanor, M. Athenes, and F. Calvo, Eur. Phys. J. B. **53**, 47 (2006).

30 P. Welch and M. Muthukumar, .Phys. Rev. Lett. **87**, 218302 (2001).

31 N. Go and H. A. Scheraga, Macromolecules, **9**, 535 (1976).

32 A. Kitao, S. Hayward, and N. Go, Proteins, **33**, 496 (1998).

33 A. Kitao and N. Go, Curr. Opin. Struct. Biol, **9**, 164 (1999).

34 D. A. Evans and D. J. Wales, J. Chem. Phys. **119**, 9947 (2003).

35 J. N. Onuchic, Z. Luthey-Schulten, and P. G. Wolynes, Ann. Rev. Phys. Chem. **48**, 545 (1997).

36 J.-E. Shea, J. N. Onuchic, and C. L. Brooks, III, Proc. Natl. Acad. Scie. USA, **99**, 16064, (2002).

37 P. Weinkam, C. Zong, and P. G. Wolynes Proc. Natl. Acad. Sci. USA, **102**, 12401 (2005).

38 N. Go, Ann. Rev. Biophys. Bioeng. **12**, 183 (1983).

39 J. N. Onuchic and P.G. Wolynes, Curr. Opin. Struct. Biol. **14**, 70 (2004).

40 Y. Sugita, A. Kitao, and Y. Okamoto. J. Chem. Phys. **113**, 6042 (2000).

41 M. Leitgeb, C. Schröder, and S. Boresch, J. Chem. Phys. **122**, 084109 (2005).

42 W. T. Coffey, Y. P. Kalmykov, and J. J. Waldron, *The Langevin Equation* (World Scientific, 2006).

43 R. J. Glauber, J. Math. Phys. **4**, 294 (1963).

44 N. Go, J. Stat. Phys. **30**, 413 (1983).

45 E. Shakhnovich, Curr. Opin. Struct. Biol. **7**, 29 (1997).

46 P. F. N. Faisca and R. C. Ball, J. Chem. Phys. **116**, 7231 (2002).

47 P. F. N. Faisca and R. C. Ball, J. Chem. Phys. **117**, 8587 (2002).

48 R. Zwanzig, J. Chem. Phys. **38**, 2766 (1963).

49 H.-X. Zhou and B. Bagchi, J. Chem. Phys. **97**, 3610 (1992).

50 T.-W. Nee and R. Zwanzig, J. Chem. Phys. **52**, 6353 (1970).

51 A. Papazyan and M. Maroncelli, J. Chem. Phys. **95**, 9219 (1991).

52 P. G. Wolynes, J. Chem. Phys. **86**, 5133 (1987).

53 L. E. Fried and S. Mukamel, J. Chem. Phys. **93**, 932 (1990).

54 S. S. Komath and B. Bagchi, J. Chem. Phys. **98**, 8987 (1993).

55 H.-X. Zhou, B. Bagchi, A. Papazyan, and M. Maroncelli, J. Chem. Phys. **97**, 9311 (1992).

56 A. Papazyan and M. Maroncelli, J. Chem. Phys. **102**, 2888 (1995).

57 J. N. Onuchic and P. G. Wolynes, J. Chem. Phys. **98**, 2218 (1993).

58 B. Derrida, Phys. Rev. Lett. **45**, 79 (1980).

59 B. Derrida, Phys. Rev. B. **24**, 2613 (1981).

60 J. D. Bryngelson and P. G. Wolynes, J. Phys. Chem. **93**, 6902 (1989).

61 V. B. P. Leite and J. N. Onuchic J. Phys. Chem. **100**, 7680 (1996).

62 V. B. P. Leite, L. C. P. Alonso, M. Newton, and J. Wang, Phys. Rev. Lett. **95**, 118301 (2005).

63 N. G. van Kampen, *Stochastic Processes in Chemistry and Physics* (North Holland Publishing, Amsterdam, 1981).

64 Y. Tanimura, V. B. P. Leite, and J. N. Onuchic, J. Chem. Phys. **117**, 2172 (2002).

65 N. Metropolis, A. Rosembluth, M. Rosembluth, and A. Teller, J. Chem. Phys. **21**, 1087 (1953).

66 A. Mitsutake, A. Sugita, and Y. Okamoto, Biopolymers, **60**, 96 (2001).

67 B. A. Berg and Neuhaus, Phys. Lett. B, **267**, 249 (1991).

68 B. A. Berg and T. Newhaus, Phys. Rev. Lett. **68**, 9 (1992).

69 J. Lee, J. Phys. Rev. Lett. **71**, 211 (1993).

70 J. Lee, J. Phys. Rev. Lett. **71**, 2353 (1993).

71 F. Wang and D. P. Landau, Phys. Rev. Lett. **86**, 2050 (2001).

72 F. Wang and D. P. Landau, Phys. Rev. E **64**, 056101 (2001).

73 M. Mezei, J. Comput. Phys. **68**, 237 (1987).

74 C. Bartels and M. Karplus, J. Phys. Chem. B, **102**, 865 (1998).

75 B. A. Berg and T. Celik, Phys. Rev. Lett. **69**, 2292 (1992).

76 U. H. E. Hansmann, and Y. Okamoto, J. Comput. Chem. **14**, 1333 (1993).

77 N. Urakami and M. Takasu, J. Phys. Soc.. Jpn. **65**, 2694 (1996).

78 H. Noguchi and K. Yoshikawa, J. Chem. Phys. **109**, 5070 (1998).

79 H. Okumura and Y. Okamoto, Chem Phys. Lett. **391**, 248 (2004).

80 H. Okumura and Y. Okamoto, Phys. Rev. E **70**, 026702 (2004).

81 S. Mukamel, *Pronciples of Nonlinear Optical Spectroscopy*, (ford University Press, New York, 1995).

82 Y. Tanimura and S. Mukamel, J. Chem. Phys. **99**, 9496 (1993).

83 K. Okumura and Y. Tanimura, J. Chem. Phys. **106**, 1687 (1997).

84 K. Okumura and Y. Tanimura, J. Chem. Phys. **107**, 2267 (1997).

85 Y. Tanimura, Chem. Phys. **233**, 217 (1998).

86 Y. Tanimura, J. Phys. Soc. Jpn. **75,** 082001 (2006).

87 P. Hamm, M. Lim, and R. M. Hochstrasser, Phys. Rev. Lett. **81**, 5326 (1998).

88 P. Hamm, M. Lim, and R. M. Hochstrasser, J. Phys. Chem. B **102**, 6123 (1998).

89 L.J. Kaufman, J. Heo, L.D. Ziegler, and G.R. Fleming, Phys. Rev. Lett. **88**, 207402 2002).

90 K.J. Kubarych, C.L. Milne, S. Lin, V. Astinov, and R.J.D. Miller, J. Chem. Phys. **116**, 2016 (2002).

91 A. Ma and R. M. Stratt, Phys. Rev. Lett. **85**, 1004 (2000).

92 T. L. C. Jansen, J. G. Snijders, and K. Duppen, J.Chem. Phys. **114**, 10910 (2001).

93 S. Saito and I. Ohmine, Phys. Rev. Lett. **88**, 207401 (2002).

94 J. Cao, S. Yang, and J. Wu, J. Chem. Phys. **116**, 3760 (2002).

95 Y. Nagata and Y. Tanimura, J. Chem. Phys. **124**, 024508 (2006).

96 R. R. Ernst, G. Bodenhausen, and A. Wokaun, Principles of Nuclear Magnetic Resonances in One and Two Dimensions (Clarendon, London, 1987).

97 K. Okumura, A. Tokmakoff, and Y. Tanimura, Chem. Phys. Lett. 314, 488 (1999).

98 K. Okumura, D. M. Jonas, and Y. Tanimura, Chem. Phys. **266**, 237 (2001)

99 S. Hahn, K. Kwak, and M. Cho, J. Chem. Phys. **112**, 4553 (2000).

100 Y. Nagata, Y. Tanimura, and S. Mukamel, J. Chem. Phys. **126**, 204703 (2007).

101 N. Demirdoven, M. Khalil, and A. Tokmakoff, Phys. Rev. Lett., **89**, 237401 (2002).

102 K. A. Merchant, W. G. Noid, D. E. Thompson, R. Akiyama, R. F. Loring, and M. D. Fayer, J. Phys. Chem. B **107**, 4 (2003).

103 K. F. Everitt, E. Geva, and J. L. Skinner, J. Chem. Phys. **114**, 1326 (2001).

104 Y. Tanimura and K. Okumura, J. Chem. Phys, **106**, 2078 (1997).

105 A. Ishizaki and Y. Tanimura, J. Chem. Phys. **125**, 084501 (2006).

106 Y. Suzuki and Y. Tanimura, J. Chem. Phys. Accepted.

107 I. Benjamin, P. F. Barbara, B. J. Gertner, and J. T. Hynes, J. Phys. Chem. **99**, 7557 (1995).

108 Y. Okamoto, J. Mol. Graph. Model. **22**, 425 (2004).

109 B. Bagchi and A. Chandra, Adv. Chem. Phys. **80**, 1 (1991).

110 B. U. Felderhof, J. Chem. Phys. **67**, 493 (1977).

111 R. A. Marcus, Discuss. Faraday Soc., **29**, 21 (1960).

112 A. Warshel, J. Phys. Chem. **86,** 2218 (1982).

113 A. Chandra and B. Bagchi, J. Chem. Phys. **91**, 7181 (1989).

114 A. Chandra and B. Bagchi, J. Chem. Phys. **94**, 2258 (1991).

115 A. Milischuk and D. V. Matyushov, J. Phys. Chem. A, **106**, 2146 (2002).

116 Y. Tanimura, H. Takano, and J. Klafter, J. Chem. Phys. **108**, 1851 (1998).

117 F. H. Stillinger, Science, **267**, 1935 (1995).

118 P. G. Wolynes, J. N. Onuchic, and D. Thirumalai, Science, **267**, 1619 (1995).

119 P. E. Leopold, M. Montal, and J. N. Onuchic, Proc. Natl. Acad. Sci. USA, **89**, 8721 (1992).

120 J. M. Luttinger and L. Tisza, Phys. Rev. **70**, 954 (1946).

121 D. V. Matyushov, J. Chem. Phys. **120**, 1375 (2004).

122 S. Mukamel, V. Khidekel , and V. Chernyak, Phys. Rev. E **53**, R1 (1996).

123 H. Takano and S. Miyashita, J. Phys. Soc. Jpn. **64**, 3688 (1995).

124 S. Koseki, H. Hirao, and H. Takano, J. Phys. Soc. Jpn. **66**, 1631 (1997).

125 L. D. Zusman, Chem. Phys. **49**,295 (1980).

126 H. Sumi and R. A. Marcus, J. Chem. Phys. **84**, 4272 (1986).